



HAL
open science

Towards a more effective and reliable salt crystallisation test for porous building materials: Experimental research on salt contamination procedures and methods for3 assessment of the salt distribution

Cristiana Nunes, Asel Maria Aguilar Sanchez, Sebastiaan Godts, Davide Gulotta, Ioannis Ioannou, Barbara Lubelli, Beatriz Menendez, Noushine Shahidzadeh, Zuzana Slížková, Magdalini Theodoridou

► **To cite this version:**

Cristiana Nunes, Asel Maria Aguilar Sanchez, Sebastiaan Godts, Davide Gulotta, Ioannis Ioannou, et al.. Towards a more effective and reliable salt crystallisation test for porous building materials: Experimental research on salt contamination procedures and methods for3 assessment of the salt distribution. *Construction and Building Materials*, 2021, 298, pp.123862. 10.1016/j.conbuildmat.2021.123862 . hal-03516171

HAL Id: hal-03516171

<https://hal.science/hal-03516171>

Submitted on 7 Jan 2022

HAL is a multi-disciplinary open access archive for the deposit and dissemination of scientific research documents, whether they are published or not. The documents may come from teaching and research institutions in France or abroad, or from public or private research centers.

L'archive ouverte pluridisciplinaire **HAL**, est destinée au dépôt et à la diffusion de documents scientifiques de niveau recherche, publiés ou non, émanant des établissements d'enseignement et de recherche français ou étrangers, des laboratoires publics ou privés.

1
2
3
4
5 1 **Towards a more effective and reliable salt crystallisation test for**
6 2 **porous building materials:**
7
8
9 3 **Experimental research on salt contamination procedures and methods for**
10 4 **assessment of the salt distribution**
11
12 5
13

14 6 Cristiana Nunes ^{a,*}, Asel Maria Aguilar Sanchez ^b, Sebastiaan Godts ^c, Davide Gulotta ^d, Ioannis Ioannou ^e,
15 7 Barbara Lubelli ^f, Beatriz Menendez ^g, Noushine Shahidzadeh ^h, Zuzana Slížková ^a, Magdalini
16 8 Theodoridou ⁱ
17 9

20 10 ^a Institute of Theoretical and Applied Mechanics of the Czech Academy of Sciences, Prosecká 76, 190 00
21 11 Prague, Czech Republic

22 12 ^b ETH Zürich, Institut für Baustoffe (IfB), Physical Chemistry of Building Materials, Stefano-Franscini-
23 13 Platz 3, 8093 Zurich, Switzerland

24 14 ^c Royal Institute for Cultural Heritage (KIK-IRPA), Jubelpark 1, 1000 Brussels, Belgium

25 15 ^d Getty Conservation Institute, 1200 Getty Center Drive, Los Angeles, CA 90049, United States

26 16 ^e University of Cyprus, 1 University Avenue, 2109 Aglantzia, Cyprus

27 17 ^f Delft University of Technology, Faculty of Architecture, Julianalaan 134, 2628 BL, Delft, The Netherlands

28 18 ^g CY Cergy Paris University, Geosciences and Environment Cergy, 1 rue Descartes, 95000 Neuville sur Oise,
29 19 France

30 20 ^h University of Amsterdam, Institute of Physics, Science Park 904-1098XH Amsterdam, The Netherlands

31 21 ⁱ Newcastle University, Hub for Biotechnology in the Built Environment, Devonshire Building, NE1 7RU
32 22 Newcastle upon Tyne, United Kingdom
33 23
34 24
35 25

36 26 * Corresponding author.

37 27 *E-mail addresses:* nunes@itam.cas.cz (C. Nunes), aselaguilars@ifb.baug.ethz.ch
38 28 (A.M. Aguilar Sanchez), sebastiaan.godts@kikirpa.be (S. Godts), dgulotta@getty.edu (D. Gulotta),
39 29 ioannis@ucy.ac.cy (I. Ioannou), b.lubelli@tudelft.nl (B. Lubelli), beatriz.menendez@cyu.fr (B.
40 30 Menendez), N.Shahidzadeh@uva.nl (N. Shahidzadeh), slizkova@itam.cas.cz (Z. Slížková),
41 31 magdalini.theodoridou@newcastle.ac.uk (M. Theodoridou)
42 32
43 33
44 34
45
46
47
48
49
50
51
52
53
54
55
56
57
58
59
60
61
62
63
64
65

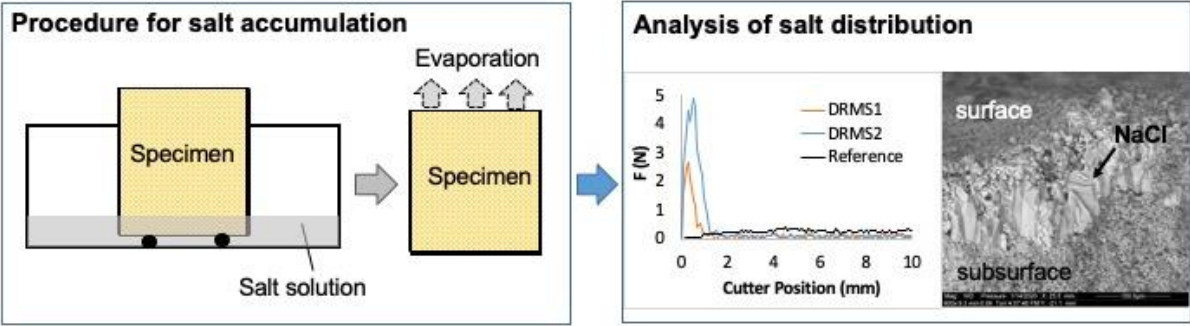
1
2
3
4
5
6
7
8
9
10
11
12
13
14
15
16
17
18
19
20
21
22
23
24
25
26
27
28
29
30
31
32
33
34
35
36
37
38
39
40
41
42
43
44
45
46
47
48
49
50
51
52
53
54
55
56
57
58
59
60
61
62
63
64
65

Abstract

The RILEM TC ASC-271 is developing a new laboratory test to assess the durability of porous building materials to salt crystallisation. The test encompasses two phases: salt accumulation and damage propagation. This paper focuses on designing a procedure for the accumulation phase; this is considered successful when salts crystallise at the material's evaporative surface (common situation observed on site) without the occurrence of damage. Two procedures were developed and tested on two limestones with different porosity: (1) capillary absorption of a salt solution followed by drying, and (2) continuous capillary absorption. Sodium chloride or sodium sulphate solutions were used. Several methods for assessing the salt distribution were employed: ultrasonic pulse velocity, drilling/scratching resistance, hygrosopic moisture content, ion chromatography, scanning electron microscopy, and micro X-ray fluorescence. The results enabled the selection of the most effective protocol for the salt accumulation phase.

Keywords: salt crystallisation test; porous materials; salt accumulation; salt distribution

Graphical Abstract



1
2
3
4 53 **1. Introduction**

54 Salt crystallisation is one of the most recurrent damage processes affecting porous building materials
55 worldwide. The durability of building materials with respect to salt crystallisation is often assessed by
56 performing accelerated weathering tests. According to Alves et al. [1], salt weathering tests are the most
57 frequent ageing tests performed in the laboratory, reflecting their worldwide importance for conservation
58 and new construction. A recent literature review on this subject [2] reports a significant variation in the
59 weathering procedures used by researchers. Despite the availability of a European standard [3], three
60 RILEM recommendations [4], [5], [6], and a guideline [7], a widely accepted and reliable salt weathering
61 test is still lacking. The use of different test procedures hinders the comparison between the results of
62 different studies.

63 To tackle this problem, in 2016, the RILEM Technical Committee ASC-271 "Accelerated laboratory test for
64 the assessment of the durability of materials with respect to salt crystallisation" (henceforth referred to
65 as TC ASC-271) was launched to develop an effective laboratory weathering test. The test should reliably
66 assess the durability of porous building materials against salt crystallisation within a reasonable period,
67 accelerating the deterioration process without significantly altering its mechanism. Since reliable
68 accelerated test procedures for simulating sea-salt spray are already available, e.g., [8], [9], the work of
69 TC ASC-271 focuses on developing a procedure that simulates salt damage triggered by capillary transport
70 of salt solution towards the evaporative surface of a material.

71 TC ASC-271 proposes a new approach to salt crystallisation tests, which differs from existing weathering
72 procedures in this field. In this approach, which is derived from the field of concrete durability [10], as
73 described in Flatt et al. [11], the salt crystallisation damage process consists of two phases: (i) the
74 induction phase, in which salts accumulate in the pores of the material (but the degree of pore filling is
75 not high enough to initiate damage); and (ii) the propagation phase, during which
76 dissolution/crystallisation cycles lead to (increasing) damage (Figure 1).

77 Starting from this approach, the new salt crystallisation test, under development by the TC ASC-271,
78 consists of two phases: (1) salt accumulation phase and (2) damage propagation phase. By this approach,
79 not adopted in existing salt crystallization procedures, it is possible to define the risk of decay due to
80 dissolution/crystallization cycles, depending on the salt content (and thus the degree of pore filling)
81 accumulated in the first stage. By separating the two phases, a better understating and forecast of the
82 decay can be achieved.

83 This paper aims to design the procedure to be followed in the accumulation phase of the salt
84 crystallisation test under development by the TC-ASC-271. The second phase of the test, i.e., the damage
85 propagation phase, is not addressed in this paper. The accumulation phase can be considered successful
86 if it enables the accumulation of salts at the material's evaporative surface (because this is the most
87 common situation observed on site) without the occurrence of damage (damage should only start in the
88 propagation phase).

89 For the assessment of the capability of the accumulation procedure to fulfil the requirement mentioned
90 above, it is crucial to measure the salt distribution in the specimen at the end of the accumulation phase.
91 This has been done with several methods (destructive and non-destructive), and their advantages and
92 disadvantages are critically discussed.

93

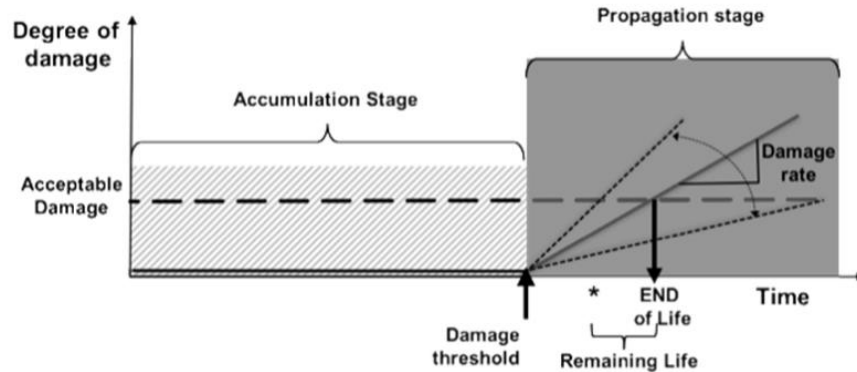


Figure 1: Schematic representation of durability of a stone, subject to salt damage, adapted from the concept proposed by Tuutti [10] to describe the durability of reinforced concrete (image from [11] provided by Robert J. Flatt (ETH Zurich)).

An extensive literature review of different salt crystallization procedures done by the TC ASC-271 is given in [2]. Standardized tests and procedures proposed by researchers can be classified into two main groups [2]:

- Contamination by capillary absorption or full immersion in a salt solution, followed by drying through one or more evaporative surfaces, e.g., [3], [4], [5], [6], [13], [14], [15], [16], [17], and
- Contamination by continuous capillary absorption of a salt solution and simultaneous drying, the so-called wick action, e.g., [18], [19], [20], [21].

In the present work, total immersion of the specimen in salt solution was not tested because it was considered not representative of the salt weathering mechanism occurring in natural exposure conditions [22]. Moreover, full immersion would not be suitable for assessing materials treated with surface treatments or for a combination of materials, such as brick/stone/plaster combinations [2]. Regarding the partial immersion procedure, the contamination can be done repeatedly with salt solution [e.g., 3] or by introducing salts only in the first cycle, followed by rewetting with pure water [e.g., 23]. In the present work, the partial immersion test considered both cases. However, rewetting with pure water was done to mobilize the salts towards the evaporative surface and not to propagate damage.

Existing standards and recommendations prescribe the use of single salt solutions [3], [4], [5], [6], usually sodium sulphate or sodium chloride, though, in natural exposure conditions, mixtures of salts prevail. Some researchers choose the composition of the salt mixture based on the analysis of salts present in the building materials on site to reproduce better a specific field condition [24], [25]. However, a standard test can hardly consider the use of salt mixtures because this would require different thermohygro-metric conditions to make it effective in other materials, which would make impossible any direct comparisons. Moreover, the action of single salts can prove more aggressive than salt mixtures [26], [27]. Hence, the present work considers the use of single salt solutions, following existing standards and recommendations.

The salt solution concentration plays a crucial role in the type and severity of damage [28]. The use of solutions with a very high salt content is common in salt crystallisation tests but can lead to unrealistic damage types and severity, e.g., [29]. The KIK-IRPA database encompassing more than six thousand samples collected from buildings in Belgium records salt contents of ca. 1 to 2 wt.% with respect to the dry weight of the sample collected onsite [30]. Therefore, in the present study, a realistic amount of salt was introduced in both materials tested (1 wt.% of the dry weight of the stones).

1
2
3
4
5
6
7
8
9
10
11
12
13
14
15
16
17
18
19
20
21
22
23
24
25
26
27
28
29
30
31
32
33
34
35
36
37
38
39
40
41
42
43
44
45
46
47
48
49
50
51
52
53
54
55
56
57
58
59
60
61
62
63
64
65

128 The most common methods for the assessment of salt damage in laboratory tests consist of visual and
129 photographic examination and mass loss determination [3], [4], [5], [6]. Mass loss is a standard method
130 for assessing damage in durability experiments and has also been used as a parameter for evaluating salt
131 crystallisation durability estimators by several authors, e.g., [15], [31], [32]. However, this method does
132 not allow obtaining information on damage and salt distribution inside the specimens. To this scope, other
133 methods and techniques can be used.

134 Ultrasonic pulse velocity (UPV) measurement is a simple non-destructive technique used to evaluate the
135 physicomaterial properties and the extent of weathering of building materials. UPV can provide
136 information about dynamic mechanical properties, porosity, and the presence of discontinuities in the
137 material [33]. As a result of the salts filling the pores, an increase of the UPV is recorded [34], so this
138 technique can be used to assess salt distribution non-destructively. The drilling resistance measurement
139 system (DRMS) and the scratch tool (ST) are micro-destructive techniques that have been used
140 successfully to monitor the salt crystallisation front in salt weathered limestone, both in the laboratory
141 and in situ, by recording increased cutting resistances in areas where pore clogging due to salt
142 crystallisation occurred [21], [35]. The ST uses a diamond cutter to make a scratch (groove) on the surface
143 of the specimen while the cutting force is recorded. The resistance of the material to cutting is related to
144 its physicomaterial properties; in fact, the intrinsic specific energy, which is the energy required for
145 scratching a unit volume of material, is directly proportional to the uniaxial compressive strength of the
146 material [36]. The DRMS operation is similar to the ST, but instead of linear cutting, the DRMS employs
147 rotational cutting (drilling).

148 Soluble salts are generally hygroscopic, i.e., they can adsorb moisture from the air when the relative
149 humidity (RH) is higher than the RH of equilibrium of the salt. In contrast, most building materials are only
150 weakly hygroscopic. Therefore, by measuring the hygroscopic moisture content (HMC) of a material at
151 high humidity, an indication of the presence of soluble salts can be attained. In the case of single salts, the
152 water activity is known; thus, a fixed relation between the salt content and the HMC at equilibrium can
153 be readily determined at a specific temperature [37], [38]. In the case of a salt mixture, several RH
154 equilibrium values are possible, which shift depending on the ionic composition [39]. The HMC method
155 uses powder drilled samples, so it can be combined with the DRMS method, provided that the drilling is
156 performed at different depths within the same drilling hole.

157 The determination of the salt content within building materials in practice usually consists of extracting
158 the soluble salts with water and analysing the ion content of the leached solution. For a semi-quantitative
159 evaluation of the salts, the HMC method can be used, whereas ion chromatography identifies the ions
160 and provides an accurate quantitative analysis [38].

161 μ -X-ray fluorescence mapping is an elemental technique that allows examining small specimen areas and
162 the production of elemental maps, with a spatial resolution on the micrometre scale. It can provide the
163 excitation of at least one measurable characteristic X-ray peak for all periodic table elements with an
164 atomic number higher than 11. Hence, the method can be applied to detect common ions present in
165 soluble salts affecting building materials, e.g., chloride (atomic number: 17) and sulphur (atomic number:
166 16). The direct observation of specimens with SEM enables examining the spatial distribution, the
167 morphological character of the salt crystals, and the size of pores in which the salt preferentially
168 crystallizes.

169 The techniques mentioned above have been used in the present study to evaluate the effectiveness of
170 the designed contamination procedures in accumulating salts close to the evaporative surface. The
171 effectiveness of the methods used is hereby critically discussed.

1
2
3
4 172 **2. Experimental**

5
6 173 **2.1. Contamination procedures**

7
8 174 Two types of salt contamination procedures have been selected for this study and are described in detail
9 175 below. A scheme depicting the two procedures is shown in Figure 2. After the accumulation phase tests,
10 176 the specimens were split into two halves for the analysis described in section 2.2., except for the
11 177 specimens subjected to UPV measurements.

12
13 178 ***P1) Capillary absorption followed by drying***

14
15 179 In this procedure, the specimens were first contaminated from the bottom by capillary absorption with a
16 180 salt solution, followed by drying only through the top surface at 20°C and 10% RH, until 80 wt.% of the
17 181 solution evaporated (Figure 2.a). Two additional wetting/drying cycles with pure water (with the same
18 182 amount of water used in the salt contamination step) were carried out to move the salts even closer to
19 183 the evaporative surface.

20
21
22 184 For both the salt contamination and rewetting steps, the salt solution (or water) was poured into a
23 185 contamination dish with glass rods. The bottom surface of the specimen was placed in contact with the
24 186 solution until the top surface was completely wet. After contamination or rewetting, the bottom of the
25 187 specimen was sealed with parafilm, and the specimen was left to dry only through the top surface.

26
27 188 The quantity of solution (or water) used was similar to the capillary moisture content, i.e., the amount of
28 189 water absorbed by the specimen at satiation (i.e., to wet the top surface), following capillary rise from its
29 190 bottom. As mentioned, the concentration of the solution was calculated so that, for both stones, a content
30 191 of 1 wt. % of salt with respect to the dry weight of the specimens was reached. Hence, a salt solution
31 192 concentration of 6.7 wt.% was used for Migné stone, and 3.8 wt.% was used for Maastricht stone.

32
33
34 193 This procedure was performed with three groups of three specimens of each stone to assess the effect of
35 194 subsequent wetting/drying cycles on salt accumulation:

- 36 195 1) a group of three specimens was subjected only to one drying cycle, following salt contamination;
37 196 specimens contaminated according to this test are henceforth referred to as **P1-1S**;
38 197 2) a group of three specimens was subjected to salt contamination, followed by one rewetting step
39 198 with water and subsequent drying; specimens contaminated according to this test are henceforth
40 199 referred to as **P1-1W**; and
41 200 3) a group of three specimens was subjected to salt contamination, followed by two rewetting steps
42 201 with water and subsequent drying; specimens contaminated according to this test are henceforth
43 202 referred to as **P1-2W**.

44
45
46 203 At the end of the tests, the specimens were further dried at 60°C in a ventilated oven to constant mass
47 204 before assessing the salt distribution.

48
49
50 205 ***P2) Continuous capillary absorption***

51
52 206 In this procedure, the salt solution was poured into a contamination dish with a geotextile layer on the
53 207 bottom (ca. 1 mm thick), and the bottom of the specimen was placed in contact with the solution (Figure
54 208 2.b). The amount of water used in the preparation of the solution was the same as the total amount of
55 209 water used in procedure P1-2W, i.e., the sum of water used during the initial salt contamination (P1-1S)
56 210 plus the water used in the two following rewetting cycles to achieve the same amount of salt (1 wt.%)
57 211 with respect to the dry weight of the specimens.

Drying occurred only through the top surface of the specimen at 20°C and 10% RH. Evaporation of the solution from the dish during the test was prevented by covering it with a parafilm sheet. After complete absorption of the salt solution, the bottom of the specimens was sealed, and the specimens were left to dry (20°C and 10% RH) until 80 wt.% of the water absorbed evaporated. Afterwards, the specimens were dried at 60°C to constant mass before assessing the salt distribution.

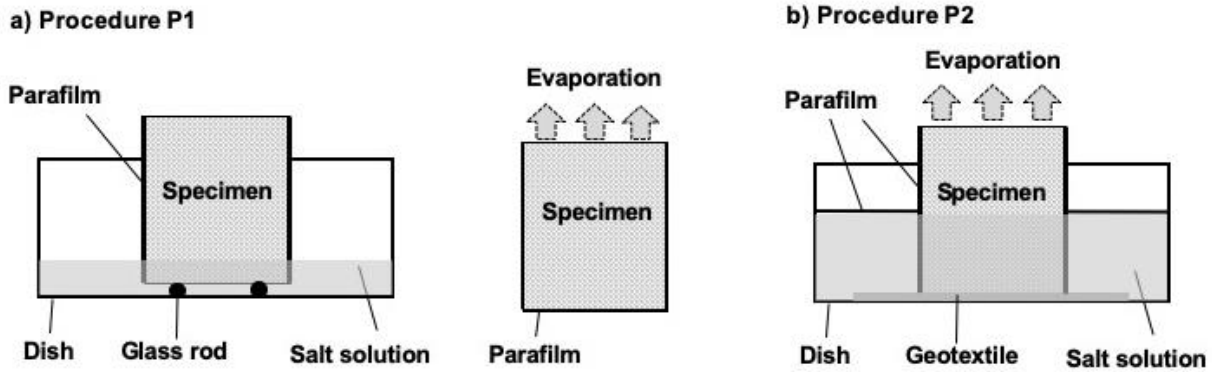


Figure 2: Experimental setup used in the contamination experiments: (a) capillary absorption followed by drying (P1), (b) continuous capillary absorption (P2).

2.2. Materials

Salt types

Two salt types, sodium chloride (NaCl) and sodium sulphate (Na₂SO₄), have been used. This selection was based on the following criteria:

- Both salts are commonly found in buildings worldwide and are known to cause severe damage.
- These salts have different crystallisation behaviour. Na₂SO₄ has temperature-dependent solubility and multiple polymorphs (hydrate and anhydrous forms) at ambient temperature. In contrast, NaCl solubility is almost independent of temperature, and NaCl has no hydrate forms at temperatures higher than 0°C.

Na₂SO₄ is generally more damaging than NaCl in laboratory weathering tests. Moreover, these salts are the most commonly used in crystallisation tests [2].

Stone types

Migné stone (quarried in France) and Maastricht stone (quarried in The Netherlands) were used in the tests. These limestones have been chosen because of their similar chemical composition (both stones are composed of ca. 95-99% of calcite), their homogeneous structure without macroscopically evident bedding planes, their unimodal pore size distribution, and their significantly different porosity and pore size. Table 1 presents the main physical properties of the stones. The open porosity of Migné is ca. 30% and that of Maastricht is ca. 50%. The grain size is homogeneous: ca. 100-150 µm for Maastricht and 1-5 µm for Migné. Maastricht has a main pore size of ca. 30 µm, whereas Migné has a main pore size of ca. 1 µm. The difference in pore size is reflected in the rate of water absorption by capillarity: Maastricht's water absorption coefficient is an order of magnitude higher than that of Migné [12].

Table 1: Properties of Migné and Maastricht limestones [12].

| Properties | Maastricht | Migné |
|------------|------------|-------|
|------------|------------|-------|

| | | |
|---|-------------|-------------|
| Open porosity (%) | 53.1 ± 0.4 | 32.4 ± 0.5 |
| Main pore size - Hg volume (µm) | 30.4 ± 0.2 | 0.95 ± 0.05 |
| Water absorption capillary coefficient (g/cm ² /min ^{0.5}) | 2.19 ± 0.16 | 0.23 ± 0.01 |

Specimen preparation and testing conditions for both procedures

Cylindrical specimens (Ø 50 mm, height 50 mm) were cut from a large stone block in such a way that the bedding planes of the stone laid parallel to the top and bottom surfaces of the specimen. The specimens were sealed along their side surface with parafilm after pre-heating them in an oven at 50°C for 10 min to achieve better adherence. A textile tape was used to glue the end of the parafilm foil and ensure sealing tightness during the entire test. Before contamination, the specimen mass was stabilized at 20°C and 10% RH, which were the conditions used during the contamination and drying phases. Low temperature, RH, and negligible air flow conditions were set to promote the accumulation of salt close to the evaporative surface.

For each procedure, a group of three specimens of each stone was contaminated with a salt solution of NaCl and another group with Na₂SO₄; both salts were ACS reagents ≥99.0%. The concentration of the salt solution used for the contamination was defined according to the desired salt content in the specimen, which was 1 wt.% of its dry weight. The same salt content was used in both procedures to enable direct comparison of the results.

A ventilated climatic chamber (Vötsch VC 4018) was used to provide constant thermo-hygrometric conditions. Throughout the tests, the specimens were placed in the climatic chamber inside plastic boxes (40×34×17cm, three specimens per box), with the opening covered with Japanese silk paper (ca. 15 g/m²) to prevent air flow. Digital thermo-hygrometers (Comet S3621) were placed inside the boxes to monitor the RH, which resulted in being 13 ± 3%.

2.3. Assessment of damage and salt distribution

At the end of the accumulation phase, the occurrence of damage and salt efflorescence was visually and photographically recorded. During the accumulation phase, the salt introduced should remain in the specimens, i.e., not crystallise as salt efflorescence, and damage should ideally be absent or of low intensity. Hence, both the amount of salt efflorescence and mass loss were used to assess the suitability of the procedures to be used in the accumulation phase.

Several analytical methods (destructive and non-destructive) were used to assess the salt distribution: ion chromatography (IC), hygroscopic moisture content (HMC), micro X-ray fluorescence (µ-XRF), scanning electron microscopy (SEM), drilling resistance measurement system (DRMS), scratch tool (ST), and ultrasonic pulse velocity (UPV).

After the accumulation phase tests, the specimens were split into two halves, using a hammer and chisel, for analysis with the mentioned methods, except for the specimens subjected to UPV measurements. Figure 3 shows a scheme summarizing the number and type of specimens and respective analyses performed with each method of assessment of salt distribution.

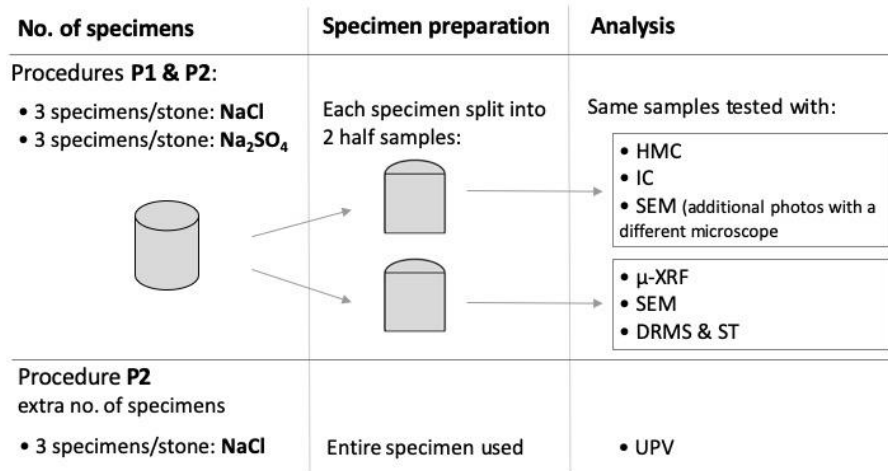


Figure 3: Summary of the number and type of specimens tested with each procedure and analysis performed.

2.3.1. Visual observations and mass variation

The development of salt efflorescence and damage was monitored photographically. Since salt efflorescence can hide the underlying damage, photographs were taken before and after removing the efflorescence. The type and severity of damage types, when present, were described according to the ICOMOS glossary [40] and MDCS atlas [41].

The weight of the specimens was recorded before and after salt contamination; based on this, the exact amount of salt introduced in each specimen was calculated. During the drying phase of both procedures, the weight of the specimens was recorded at regular intervals until 80 wt.% of the water had evaporated. The damage was assessed by recording the mass loss.

At the end of the test, the salt efflorescence and stone debris, when present, were collected using a soft brush and weighed using a balance (resolution of 10^{-4} and accurate to 10^{-3} g). The salt efflorescence was separated from the stone debris by dilution in pure water, followed by filtration with filter paper. The weight of the debris was measured, and that of the salt was calculated. Salt that might have accumulated in the pores of the stone debris collected was hence registered as salt efflorescence.

2.3.2. Ion chromatography (IC)

For the analysis of the salt content (NaCl or Na₂SO₄), measurements were carried out on drilled powder samples. For each half-core specimen, starting from the evaporative surface, samples were collected up to the following depths (same hole): 0-5, 5-10, 10-15, 15-20, 20-30, 30-40, and 40-50 mm. Additionally, to get more precise information on the salt distribution in the salt-rich outer layer, samples were collected by sanding down a half-cylinder at 1 mm intervals up to 5 mm depth per specimen.

The quantity of anions (Cl⁻ and SO₄²⁻) and cations (Na⁺) of the vacuum filtered extract was analysed by IC (Metrohm). The results in parts per million (ppm – mg/L) were converted to wt.% (relative to the dry sample weight), and the sum of the equimolar contents of Na⁺ and Cl⁻ or SO₄²⁻ was estimated. The salt amount present in each layer was calculated as the percentage of the total salt content present in the sample. The average amount of each ion (in wt.%) in each group of three specimens contaminated with each procedure was calculated in relation to the respective total weight of each group of samples.

2.3.3. Hygroscopic Moisture Content (HMC)

For the determination of the HMC, the same samples used in the IC analysis were placed in a climate chamber at 20 (± 1) °C and 95% (± 3) RH until constant weight (41 days). The HMC was calculated according to the equation:

$$HMC = 100 \cdot \frac{\Delta m}{m_d} \quad (1)$$

in which Δm represents the mass gain of the sample (g), and m_d represents the dry weight of the sample (g).

The correlation between the HMC values (wt.%) and the salt content (wt.%) was determined considering a dataset of 292 drilled samples. The salt content considered was limited to equimolar contents derived from the IC analysis of samples containing Na⁺ and Cl⁻ or Na⁺ and SO₄²⁻. The correlation coefficient indicates how well the data fits the model of regression and is presented as R², calculated according to the following equation:

$$R^2 = \left(\frac{n(\sum xy) - (\sum x)(\sum y)}{\sqrt{[n\sum x^2 - (\sum x)^2][n\sum y^2 - (\sum y)^2]}} \right)^2 \quad (2)$$

in which x corresponds to the value of HMC (wt.%), and y corresponds to the salt content (wt.%).

2.3.4. Micro X-ray fluorescence mapping (μ -XRF)

Chloride and sulphur μ -XRF maps were produced to check the NaCl and Na₂SO₄ distribution, respectively. The instrument used for the μ -XRF analysis was an EDAX (Mahwah, NJ, USA) ORBIS μ -XRF spectrometer. The system uses a Silicon Drift Detector (SDD). It focuses the X-rays from a rhodium target anode with a poly-capillary focusing optic, which allows for a beam diameter of ca. 30 μ m. The acquisition system is the ORBIS Vision Software supplied by EDAX. The applied acceleration potential and current were 35 kV and 500 μ A, respectively. At each point, every 100 μ m (spacing), a spectrum was acquired for 100 ms (30%-40% dead time). The measurements were carried out at atmospheric conditions with a built-in 25- μ m thick aluminum filter to eliminate the rhodium L α radiation, which overlaps with the chlorine K α X-ray line and increases its limit of detection.

A smooth surface is required for this analysis, so prismatic specimens were dry-cut from the half cores along their longitudinal axis. The selected surface of 5x5 cm to be mapped was ground with SiC paper (STRUERS 500) for 15 seconds, at 300 rpm, in a single direction to avoid spreading the salt.

2.3.5. Scanning Electron Microscopy (SEM)

SEM observations were carried out on the same samples analysed with μ -XRF. Polished sections were produced from 2x2 cm pieces of stone. The samples were prepared in the same way as those prepared for the μ -XRF analysis but were further embedded under vacuum in low viscosity epoxy resin (EPO-TEK). After 24 h of polymerization, the specimens were grinded with SiC paper (STRUERS) at 500, 1000, 2400, and 300 rpm for 5 min (each step), using isopropanol as coolant. The final polishing was carried out with water-free diamond polishing suspensions (9, 3, and 1 μ m). Polished surfaces were coated with a 15 nm carbon layer, then observed with an SEM FEI QUANTA 200 3D, at high vacuum, and 20 kV voltage.

Additional samples from Maastricht limestone contaminated with Na₂SO₄ according to procedure P1-1S (belonging to the same set analysed with IC and HMC) were studied with a Zeiss Gemini 300 SEM FE equipped with an Oxford X-Max detector at high vacuum and 15 kV voltage. Polished cross-sections were prepared by embedding the stone fragments in bi-component epoxy resin (EpoFix, Struer), grinding them

1
2
3
4 345 with SiC paper (Struers), and polished with polishing cloth up to 8000 grit. Isopropanol was used during
5 346 grinding and polishing to avoid salt dissolution. The salt distribution within the stone matrix was mapped
6 347 up to a 2.5 mm depth from the evaporative surface by combining multiple images acquired in constant
7 348 conditions (back-scattered mode) at 150x magnification.

9 349 **2.3.6. Drilling resistance measurement system (DRMS) and scratch tool (ST)**

10 350 Samples contaminated according to procedure P1, and previously mapped with μ -XRF, were scratched
11 351 and drilled to assess the position of the salt crystallisation front. Non-contaminated Migné and Maastricht
12 352 samples were also used as a reference.

13 353 Scratching was performed using a WOMBAT Scratch Tool supplied by Epslog Engineering. The samples
14 354 were scratched along the centre of their curved side, moving from the evaporative surface towards the
15 355 base. A sharp rectangular 10 mm wide diamond cutter with a negative back rake angle of 15°, moving at
16 356 constant velocity (10 mm/s), was used in all the scratch tests. During scratching, the normal (F_n) and
17 357 tangential (F_t) components of the total force required to form a groove on the sample were recorded
18 358 automatically. From these, the total cutting force (F) was estimated as [30]:

$$19 359 F = \sqrt{(F_n^2 + F_t^2)} \quad (3)$$

20 360 For the DRMS test, the samples were drilled starting at the evaporative surface of the samples using a
21 361 device supplied by SINT Technology. The operating conditions during drilling were 600 rpm for the
22 362 rotational speed and 10 mm/min for the penetration rate. A twist diamond drill bit with a flat point and
23 363 \varnothing 5 mm was used; the total penetration depth was 10 mm. During the drilling tests, the DRMS provided
24 364 a continuous reading of the force required to perforate the test specimen.

25 365 **2.3.7. Ultrasonic pulse velocity (UPV)**

26 366 UPV measurements were performed to assess the salt distribution non-destructively, using a portable
27 367 instrument (USG 20 Krompholz Geotron Elektronik (DE)) with pointy-ended transducers with a contact
28 368 section of \varnothing 3 mm. Only specimens contaminated according to procedure P2 were measured; for this test,
29 369 three extra cylindrical specimens of each stone were used. Nine measurements were performed in each
30 370 specimen in planes parallel to the evaporative surface at 5 mm intervals. The measurements were
31 371 performed before and after salt contamination.

32 372 **3. Results**

33 373 **3.1. Damage and salt efflorescence**

34 374 A summary of the visual observations, focusing on the qualification of salt efflorescence and damage on
35 375 the specimens contaminated with both procedures, is shown in Figures 4 and 5. The amount of salt
36 376 efflorescence and mass loss are given in Figures 6 and 7, respectively. In the case of procedure P1, the
37 377 debris of the specimens subjected to further rewetting steps was only collected at the end-step, so the
38 378 results shown are cumulative.
39 379

40 380 Samples contaminated with NaCl with both procedures developed only salt efflorescence, and no visible
41 381 damage was detected (Figure 4). The type and amount of salt efflorescence (Figure 6.a) varied according
42 382 to the procedure followed and type of stone used: a lower amount of NaCl efflorescence developed in the
43 383 less porous stone (Migné) with procedures P1-1S and P2, but the amount was still slightly higher than for
44 384 the more porous stone (Maastricht) with procedures P1-1W and P1-2W. The results of mass loss (Figure
45 385 7.a) can be considered negligible (lower than 0.05 wt.%) and confirm the visual observations.

1
2
3
4
5
6
7
8
9
10
11
12
13
14
15
16
17
18
19
20
21
22
23
24
25
26
27
28
29
30
31
32
33
34
35
36
37
38
39
40
41
42
43
44
45
46
47
48
49
50
51
52
53
54
55
56
57
58
59
60
61
62
63
64
65

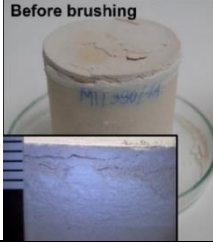
Both types of stones contaminated with Na₂SO₄ showed damage with all procedures (Figure 5). Minor damage was observed in Migné after Na₂SO₄ contamination with procedure P1-1S, leading to ca. 1 wt.% of mass loss (Figure 7.b); the amount of salt efflorescence observed was very low and concentrated close to the evaporative surface. After one rewetting, Na₂SO₄ contaminated Migné specimens (P1-1W) suffered rapid and severe damage (within 24h of drying). For this reason, the planned second rewetting was not performed, and these specimens were not subjected to the analysis of salt distribution.

In the case of the more porous stone (Maastricht), samples contaminated with Na₂SO₄ with procedure P1-1S developed slight granular disintegration and scaling, leading to 0.7 ± 0.4 wt.% mass loss (Figure 7.b). After one rewetting (P1-1W), the amount of salt efflorescence increased significantly; the amount of efflorescence reached almost 90 wt.% of the salt introduced, whereas mass loss was ca. 1.1 wt.%. The 2nd rewetting step (P1-2W) induced more damage (ca. 2 wt.% of mass loss) and slightly more salt efflorescence. In contrast with Migné, damage occurred in Maastricht samples contaminated with Na₂SO₄ with procedure P2.

| Procedure | | Migné - NaCl | Maastricht - NaCl |
|-----------|--------------------|---|--|
| P1-1S | Photo |  |  |
| | Damage/alteration | Efflorescence | Efflorescence |
| | Salt efflorescence | Powdery | (micro) cauliflower |
| | Damage severity | No damage | No damage |
| | Damage extension | - | - |
| P1-1W | Photo |  |  |
| | Damage/alteration | Efflorescence | Efflorescence |
| | Salt efflorescence | Powdery (surface) and hollow crust | Powdery |
| | Damage severity | No damage | No damage |
| | Damage extension | - | - |
| P2-2W | Photo |  |  |
| | Damage/alteration | Efflorescence | Efflorescence |
| | Salt efflorescence | Powdery | Powdery |
| | Damage severity | No damage | No damage |
| | Damage extension | - | - |

1
2
3
4 399
5 400
6 401

Figure 4: Summary of the macroscopic visual observations on the specimens contaminated with NaCl. Scores of severity of damage: low (+) to high (++++). Scores of extension of damage: small (+) to large (++++) surface area.

| Procedure | | Migné – Na ₂ SO ₄ | | Maastricht – Na ₂ SO ₄ | |
|-----------|--------------------|---|---|--|---|
| P1-1S | Photo |  |  |  |  |
| | Damage/alteration | Scaling with subflorescence | | Efflorescence, granular disintegration, and scaling with subflorescence | |
| | Salt efflorescence | Powdery | | Powdery | |
| | Damage severity | ++ | | ++ | |
| | Damage extension | ++ | | ++ | |
| P1-1W | Photo |  | |  |  |
| | Damage/alteration | Bursting with subflorescence | | Granular disintegration with subflorescence | |
| | Salt efflorescence | Crust | | Crust | |
| | Damage severity | ++++ | | ++ | |
| | Damage extension | ++++ | | ++++ | |
| P2 | Photo |  |  |  |  |
| | Damage/alteration | Efflorescence | | Contour scaling with subflorescence | |
| | Salt efflorescence | Cauliflower | | Powdery | |
| | Damage severity | + | | ++ | |
| | Damage extension | + | | ++ | |

52 402
53 403
54 404
55

Figure 5: Summary of the macroscopic visual observations on the specimens contaminated with Na₂SO₄. Scores of severity of damage: low (+) to high (++++). Scores of extension of damage: small (+) to large (++++) surface area.

65

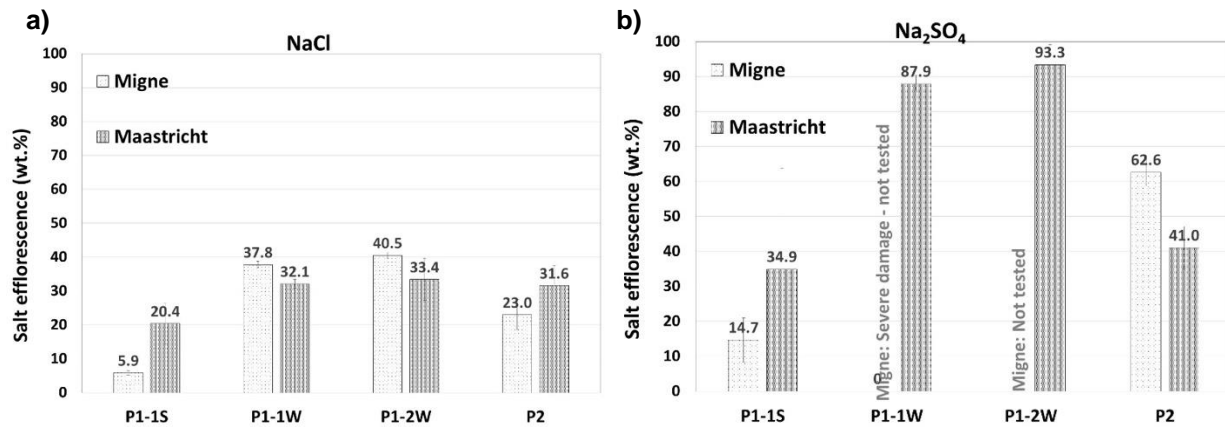


Figure 6: Mass of salt efflorescence registered after the salt accumulation test with procedures P1 and P2 expressed as the percentage relative to the total salt amount introduced in the specimens: (a) stones contaminated with NaCl, (b) stones contaminated with Na₂SO₄.

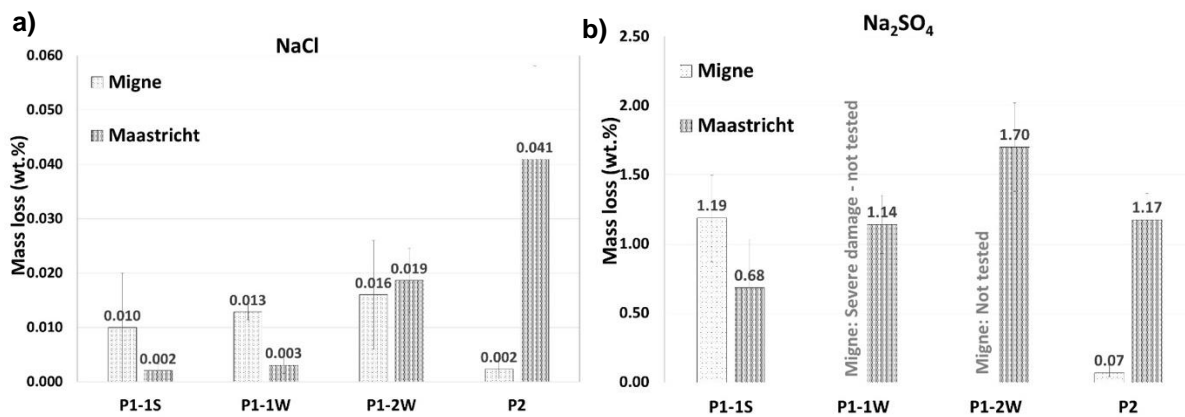


Figure 7: Mass loss of stone material registered after the salt accumulation test with procedures P1 and P2, expressed as the percentage relative to the dry weight of the specimens: (a) stones contaminated with NaCl, (b) stones contaminated with Na₂SO₄.

The period for the evaporation of 80% of the water introduced during the contamination varied according to the stone type, salt type, and procedure (Table 2). As expected, samples with higher porosity and pore size dried faster. The drying period with procedure P2 was more prolonged than with procedure P1-1S for both stones contaminated with either salt. This aspect can be attributed to the higher degree of saturation of the porous system of the stones with procedure P2, resulting from the continuous capillary absorption of a solution with two times higher amount of water than procedure P1-1S.

Table 2: Period (in days ± 3) for evaporation of 80% of the water introduced during the contamination.

| Procedure | Migné | | Maastricht | |
|-------------|-------|---------------------------------|------------|---------------------------------|
| | NaCl | Na ₂ SO ₄ | NaCl | Na ₂ SO ₄ |
| P1 -1S | 37 | 24 | 10 | 10 |
| P1 -1W & 2W | 21 | - | 8 | 8 |
| P2 | 40 | 30 | 12 | 12 |

3.2. Assessment of the salt distribution

3.2.1. Ion chromatography (IC) and hygroscopic moisture content (HMC)

The salt distribution assessed with IC is presented in Figures 8 and 9. Generally, salt accumulated close to the evaporative surface and the salt content decreased with depth. The salt content in the outer 5 mm layer was always above 50 wt.% of the total content, except in the case of **Maastricht** contaminated with **Na₂SO₄** with procedure **P1-1S** (Figure 9.b). In this case, the amount of salt present in the outer 5 mm layer was lower than ca. 30 wt.%, but the standard deviation was large.

Different results were obtained when the samples were rewetted; the salt content up to 5 mm depth slightly increased or decreased after one rewetting (**P1-1W**) for Migné and Maastricht contaminated with **NaCl**, respectively. Subsequent rewetting of Migné stone contaminated with **NaCl** (**P1-2W**) led to an increment of efflorescence and salt in the 0-5 mm layer. In Maastricht, the amount of salt efflorescence decreased with subsequent rewetting (ca. 30 wt.%), while the salt content in the 0-5 mm layer increased. **Maastricht** contaminated with **Na₂SO₄** with **P1-1W** showed an increment of the salt content in the outer layer (0-5 mm); rewetting twice (**P1-2W**) led to an increment of efflorescence and a decrease of the salt content in the outer layer. These results are possibly related to the removal of the damaged salt-rich layer after brushing the specimens contaminated with **P1-2W**. Upon rewetting (**P1-1W** and **P1-2W**), salts were transported towards the evaporative surface; consequently, the salt content in the outer 5 mm layer and/or the amount of efflorescence increased.

A more detailed analysis was carried out on the first 5 mm of a sample of **Maastricht** contaminated with **Na₂SO₄** according to procedure **P1-1S** (Figure 10). The results indicate that 73.5 wt.% of the total salt content was located within the first millimetre of the specimen. Deeper in the stone, the concentration dropped significantly, with 16.8 wt.% between 1 and 2 mm, and 2.6 wt.% between 4 and 5 mm. Considering the open porosity, bulk/skeletal density of the stone, mass of salt in the stone, molar mass/volume of thenardite or phase III, it is possible to estimate that 10 % of the volume of the pores in the outer 1 mm were filled with salt (assuming a homogeneous distribution of salt, including a thin salt crust on the surface of the sample).

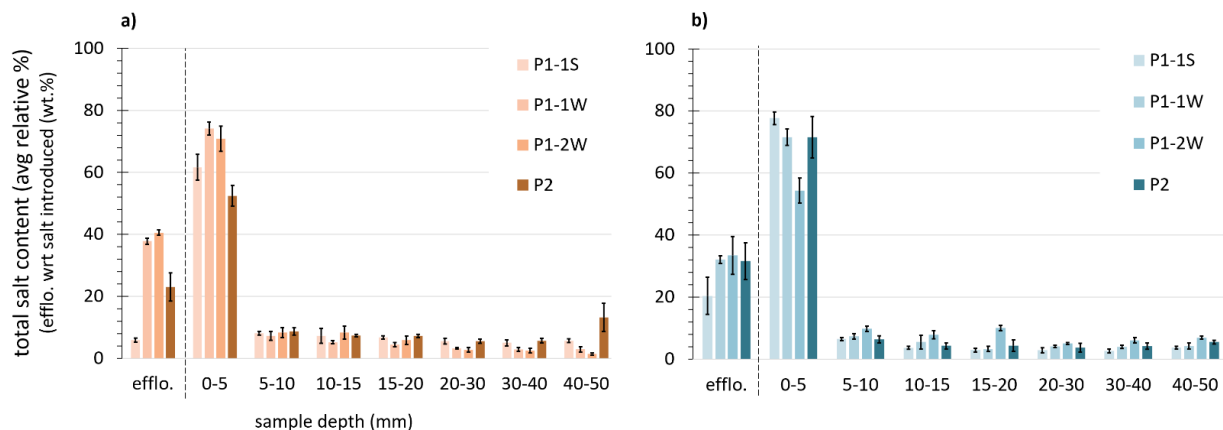


Figure 8: Mean relative percentage of NaCl distribution assessed with IC in Migné (a) and Maastricht (b) after contamination with procedures P1 and P2. The values are the average of 3 specimens; the graphs include the amount of salt efflorescence (efflo). The legend from top to bottom represents the different procedures, which sequentially correspond to the columns from left to right.

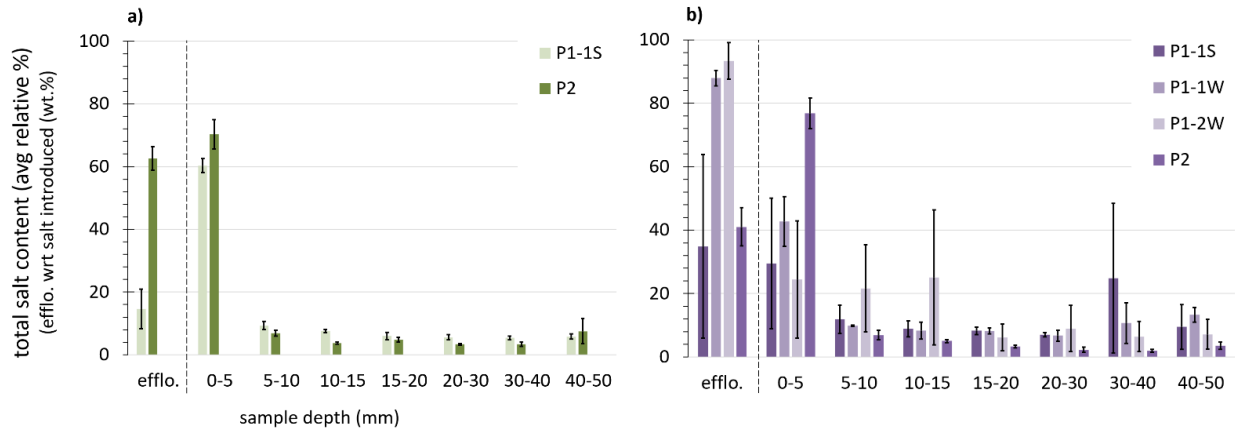


Figure 9: Mean relative percentage of Na_2SO_4 distribution assessed with IC in Migné (a) and Maastricht (b) after contamination with procedures P1 and P2. The values are the average of 3 specimens; the graphs include the amount of salt efflorescence (efflo). The legend from top to bottom represents the different procedures, which sequentially correspond to the columns from left to right.

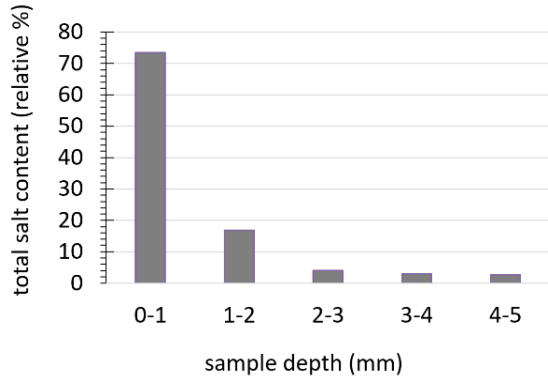


Figure 10: Relative percentage of Na_2SO_4 distribution in the first millimetres of Maastricht contaminated with procedure P1-1S.

The salt distribution results obtained with HMC are in line with those measured by IC. The correlation of determination between HMC and IC salt content was used in this study to check whether HMC could give reliable semi-quantitative results. Considering 168 samples with a wide range of salt contents (Figure 11.a), a good correlation was derived ($R^2 = 0.9305$). However, when considering a salt content below 1 wt.% (144 samples), the correlation dropped significantly ($R^2 = 0.6175$) (Figure 11.c). In samples with such a low salt content and weight (ca. 0.928 g), the experimental error increases. Next to the experimental error, minimal changes in RH in the climatic chamber can have a significant impact on the HMC values, especially in the case of high RH and hygroscopic salts, such as NaCl.

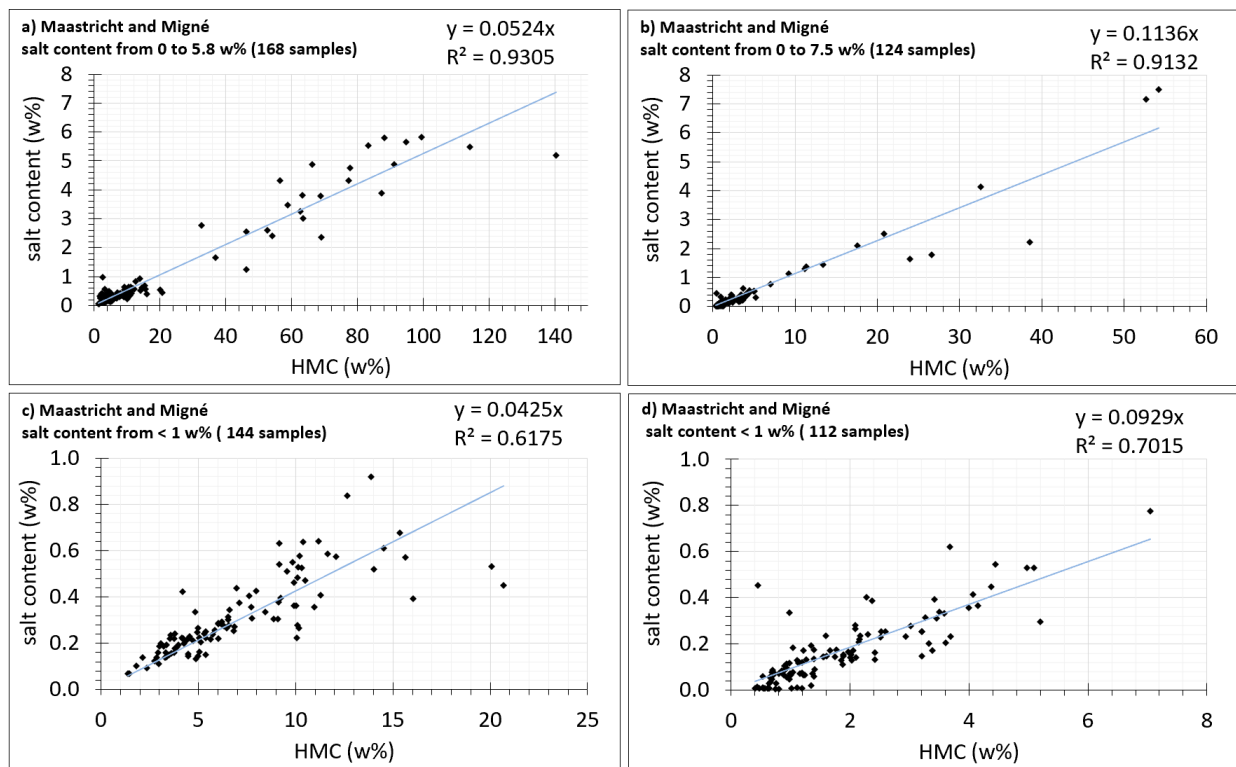


Figure 11: Correlation between HMC values and salt content (R^2 = coefficient of determination): Maastricht and Migné with NaCl (a) and Na_2SO_4 (b) content (full range detected between 0 and 5.8 or 7.5 wt.%) and with NaCl (c) and Na_2SO_4 (d) content below 1 wt.%.

3.2.2. Micro X-ray fluorescence mapping (μ -XRF) and scanning electron microscopy (SEM)

A summary of the observations from μ -XRF maps and SEM images is presented in Table 3. Figure 12 gives an example of the μ -XRF maps recorded in Migné and Maastricht contaminated according to procedure P1 with NaCl. Figures 13, 14, 15, and 16 show a few selected SEM microphotographs.

The results indicate that procedure **P1-1S** is the most effective in accumulating salt at the evaporative surface of both stones. In general, rewetting reduces the thickness of the salt layer and promotes the redistribution of salts deeper into the samples. The data also indicated that NaCl is more prone to be redistributed within the sample thickness of both stones upon rewetting. Procedure **P2** also showed a salt layer at the evaporative surface in both stones, with either salt; NaCl further spread within the sample thickness.

SEM gives a more precise assessment of the thickness of the salt layer and salt distribution than the μ -XRF maps, although the salt distribution can be quite non-homogeneous. Therefore, a thickness interval is probably more appropriate rather than a single value. The representativeness of the sample observed with SEM can also be an issue; e.g., no salt layer was observed under SEM with Maastricht contaminated with procedure P1-1S with NaCl, but a salt layer up to 1 mm thickness was observed in the μ -XRF maps.

491 **Table 3:** Summary of μ -XRF maps and SEM image observations.

| Procedure | Method | Migné - NaCl | Maastricht - NaCl | Migné – Na ₂ SO ₄ | Maastricht – Na ₂ SO ₄ |
|-----------|-----------------|---|---|---|--|
| P1-1S | μ -XRF maps | - Cl layer up to 1 mm depth (Figure 12.a) - Cl dispersed throughout the sample (Figure 12.b) | - Cl layer up to 1 mm depth | - S layer up to 1 mm depth | - S layer up to 1 mm depth |
| | BSE images | - Salt layer up to 200-500 μ m depth (Figure 14) | - No salt layer observed - Scattered salt crystals | - Salt layer up to 50 μ m depth - Salt crystals up to 2 mm depth | - Salt layer up to 200 μ m depth (Figure 13) - Most of the salt up to 400-500 μ m depth. - Scattered salt crystals up to 2mm depth |
| P1-1W | μ -XRF maps | - Cl rich layer up to 1 mm depth - Cl dispersed throughout the sample with a slightly higher concentration at the bottom | - Cl rich layer up to 0.5 mm depth - Cl scattered up to 10 mm depth (Figure 12.c, d) | * | - S layer up to 1 mm depth |
| | BSE images | - Salt dense layer up to 200-250 μ m depth | - Continuous salt layer up to 400 μ m depth | * | - Salt layer up to 150 μ m depth |
| P1-2W | μ -XRF maps | - Cl layer up to 0.5 mm depth | - Cl layer up to 0.5 mm depth | * | - S was not detected |
| | BSE images | - Salt dense layer up to 200-250 μ m depth | - Non-continuous salt layer up to 200 μ m depth | * | - No salt layer observed |
| P2-2W | μ -XRF maps | - Cl layer up to 1 mm depth - Cl also dispersed up to 10 mm depth | - Cl layer up to 1 mm depth - Cl also dispersed up to 2.5 mm depth | - S layer up to 1 mm depth | - S layer up to 1 mm depth |

* Not measured (severe damage of the specimen after rewetting)

1
2
3
4
5
6
7
8
9
10
11
12
13
14
15
16
17
18
19
20
21
22
23
24
25
26
27
28
29
30
31
32
33
34
35
36
37
38
39
40
41
42
43
44
45
46
47
48
49
50
51
52
53
54
55
56
57
58
59
60
61
62
63
64
65

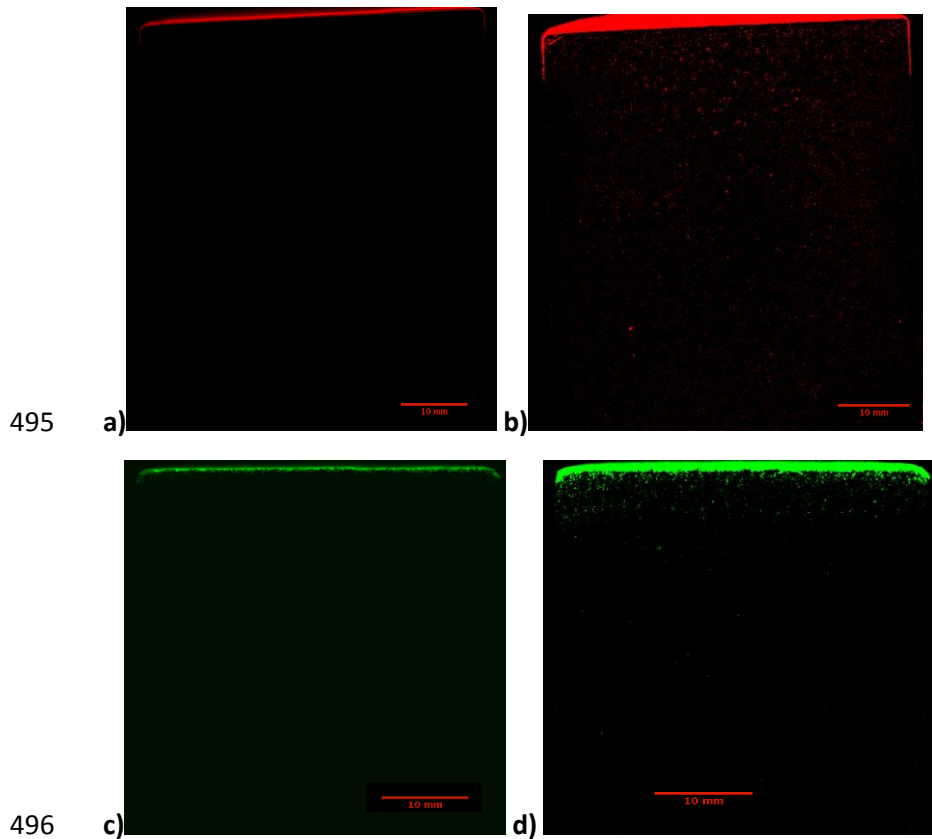


Figure 12: μ -XRF chloride maps of Migné and Maastricht contaminated according to procedure P1. Migné contaminated according to procedure P1-1S: (a) original map, (b) enhanced map by Image J software; the dense red layer on the top of the sample is an image artefact. Maastricht contaminated according to procedure P1-1W: (c) original map, (d) enhanced map by image J software; the dense green layer on the top of the sample is an image artefact.

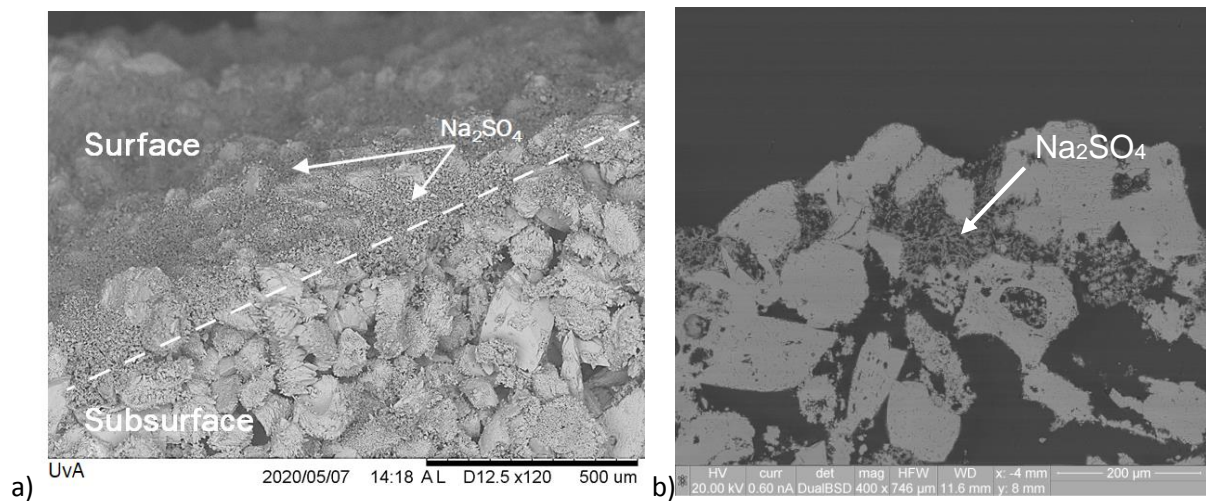
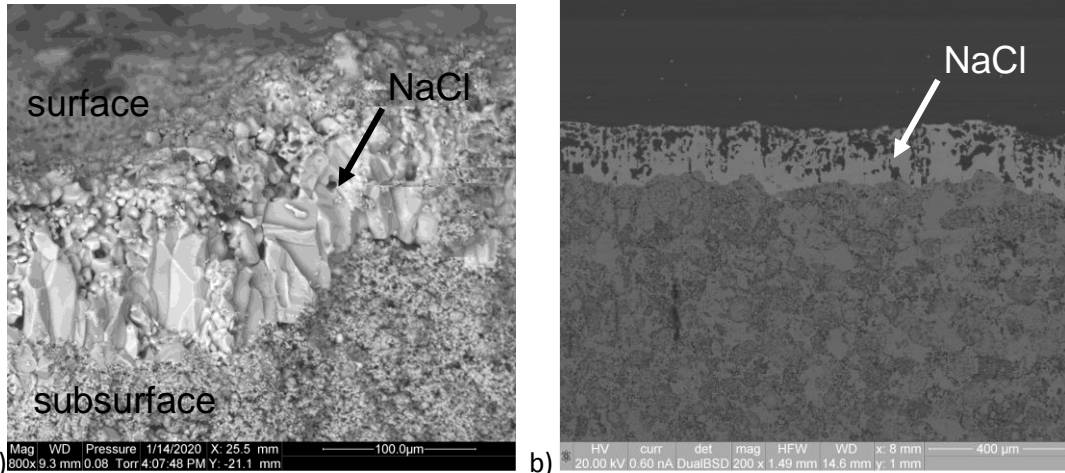
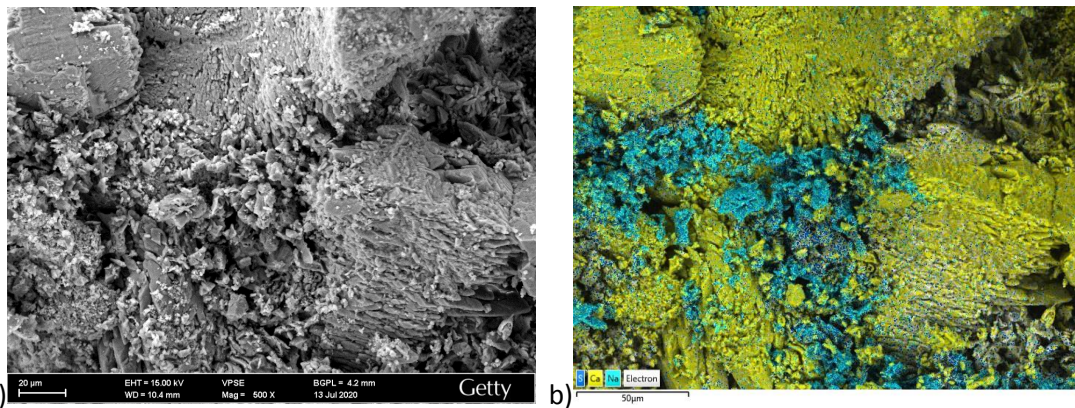


Figure 13: Maastricht contaminated with Na_2SO_4 according to procedure P1-1S: (a) SEM image of the ground surface. (b) BSE image on polished section showing a layer of Na_2SO_4 crystals filling the interparticle porosity just beneath the evaporative surface (the arrow indicates the location of salt as analysed with EDX).



507 a) 508 **Figure 14:** Migné contaminated with NaCl according to procedure P1-1W: (a) SEM image of the ground
 509 surface, (b) BSE image of the polished section.

510 The additional SEM analysis of Maastricht contaminated with Na₂SO₄ with procedure **P1-1S** showed only
 511 partial filling of the pore spaces and a higher concentration of the salt close to the evaporative surface.
 512 Images of the fresh fracture showed that the salt crystallizes as porous clusters within the inter-particle
 513 spaces (Figure 15). Such a crystallisation pattern was confirmed by the cross-section observation and
 514 mapping of the salt distribution (Figure 16). The salt was mostly concentrated up to 400-500 μm from the
 515 evaporative surface, showing a rather irregular distribution. The presence of salt was detected at least up
 516 to 2 mm depth, as isolated clusters of salt crystals formed along the grain borders of the stone. These
 517 observations are in line with the IC results on the same sample (Figure 10) in which ca. 70% of the salt was
 518 detected up to 1 mm depth and ca. 20% of salt was detected between 1.5 and 2 mm depth.



519 a) 520 **Figure 15:** SEM images of the fresh fracture close to the evaporative surface of Maastricht contaminated
 521 with Na₂SO₄ according to procedure P1-1S: (a) BSE image, (b) False colour image after EDS analysis,
 522 showing the distribution of calcium (yellow), sodium and sulphur (cyan and blue respectively).

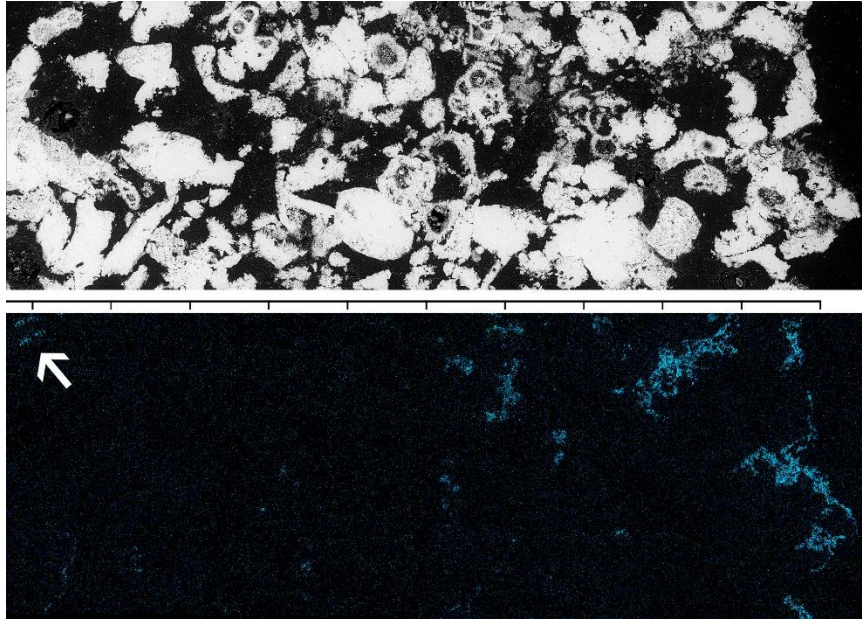


Figure 16: Maastricht contaminated with Na_2SO_4 according to procedure P1-1S. In both images, the evaporative surface is located on the right side. Above: BSE image of the cross-section. Below (same cross-section): EDS false-color map showing the salt distribution according to depth (sodium and sulphur are shown in cyan and blue, respectively; contrast has been enhanced for better clarity) with the presence of salt clusters up to 2 mm depth (arrow). Scale segments = 200 microns.

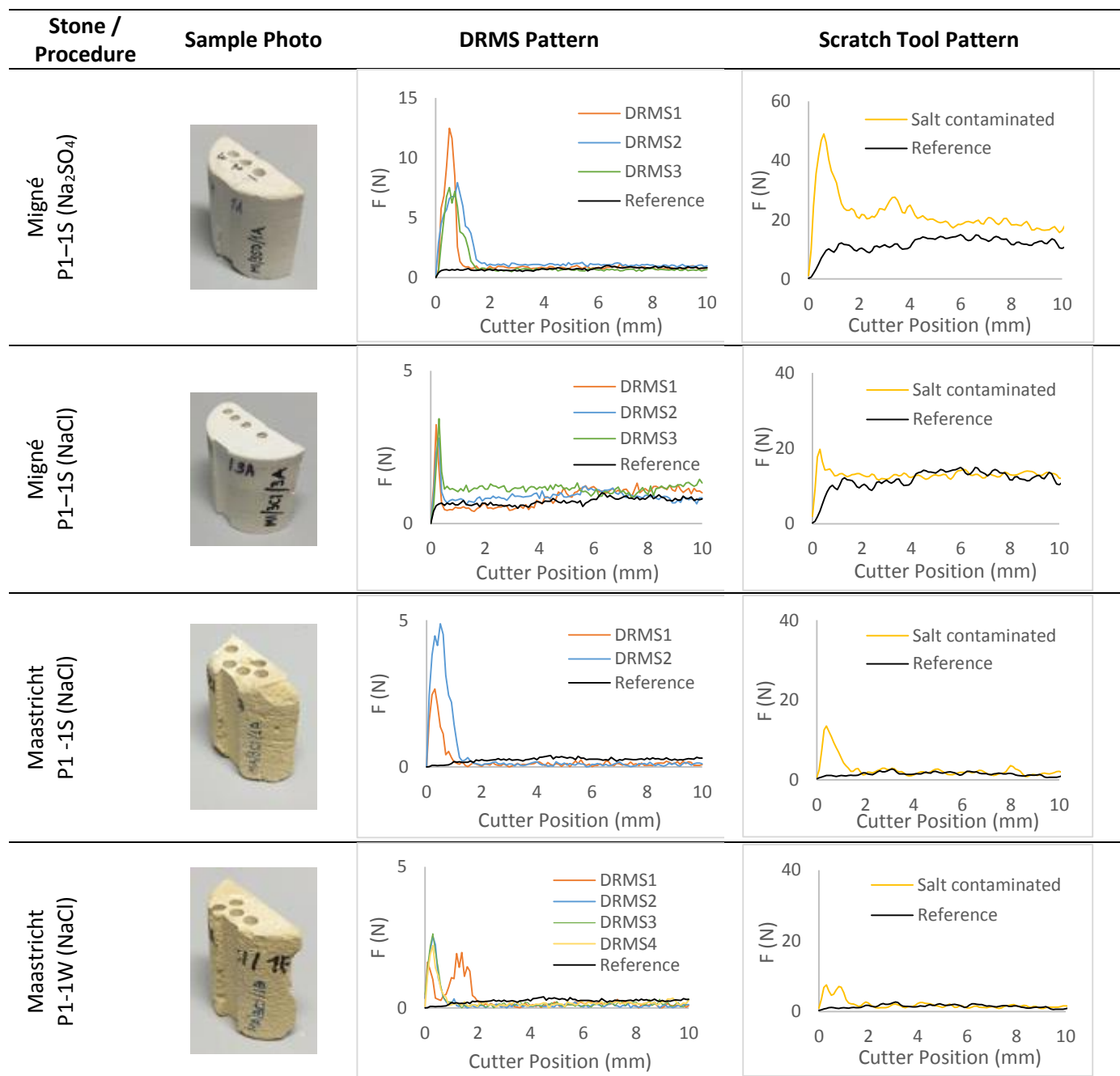
3.2.3. Drilling resistance measurement system (DRMS) and scratch tool (ST)

The scratching and drilling force (F) patterns versus the cutter position (depth of the sample) are provided in Figure 17. From these, evident changes in the microstructure of the salt contaminated samples (i.e., pore clogging resulting in increased cutting resistance areas) can be observed. In particular, in all the patterns derived after salt contamination and drying, localized peaks in material resistance to cutting were recorded very close to the evaporative surface (ca. 0 - 2 mm). These peaks, which are not observed in the reference specimens, are prominent both in the ST and the DRMS patterns and suggest pore filling by the salts.

The position of the peaks in cutting resistance is nearly identical for each sample, irrespective of the mapping technique used, indicating that both methods are detecting pore clogging due to salt crystallisation at more or less the same location. This is in line with previous applications of the ST and the DRMS [21], [29] and confirms the reliability of both techniques and their potential in detecting the position of the salt crystallisation front in limestone.

The peak cutting resistance recorded in the case of **Migné** contaminated with Na_2SO_4 with procedure **P1-1S** is much higher, compared to the corresponding sample contaminated with **NaCl**. This is in line with the μ -XRF and SEM results (Table 3), which suggest that Na_2SO_4 has a tendency to crystallise more locally, closer to the evaporative surface, as opposed to **NaCl** which shows higher dispersion. The localised crystallisation of Na_2SO_4 usually leads to more damage [16], as was indeed the case in the visual observations hereby reported (Figures 4 and 5). In the case of the much weaker and porous **Maastricht** stone, the peak resistance recorded for the sample contaminated once (**P1-1S**) with **NaCl** was again rather low. Upon rewetting with water (**P1-1W**), the peak resistance was further reduced. In contrast, the thickness of the salt-rich layer (i.e., increased cutting resistance area) appears broader, albeit not as broad

551 as in the optimised μ -XRF map, suggesting some redistribution of the salt content with water absorption
 552 and possibly some salt escaping the sample as efflorescence; this is in line with the amount of salt
 553 efflorescence formed, as well as the IC data (Figure 8).



554 **Figure 17:** DRMS and average ST patterns for samples contaminated according to procedure P1
 555 (coloured lines) and reference samples (black lines).

3.2.4. Ultrasonic pulse velocity (UPV)

The UPV results before and after contamination with **NaCl** with procedure **P2** are shown in Figure 18; the values given correspond to the percentage change before and after contamination. After salt contamination, a significant UPV increase is observed in Maastricht at 0-10 mm depth from the evaporative surface; UPV values at 5 mm increased by 44%, compared to the same specimen without salt. These results indicate that salt accumulated in the first 5 mm of the specimen. In contrast, a very slight difference in UPV values before and after salt contamination was detected in Migné stone contaminated with **NaCl**. Figure 18.b) shows only 7% UPV increase after Migné salt contamination; these results suggest that salt has evenly precipitated throughout the depth of the specimen, which is not in line with the IC and HMC results.

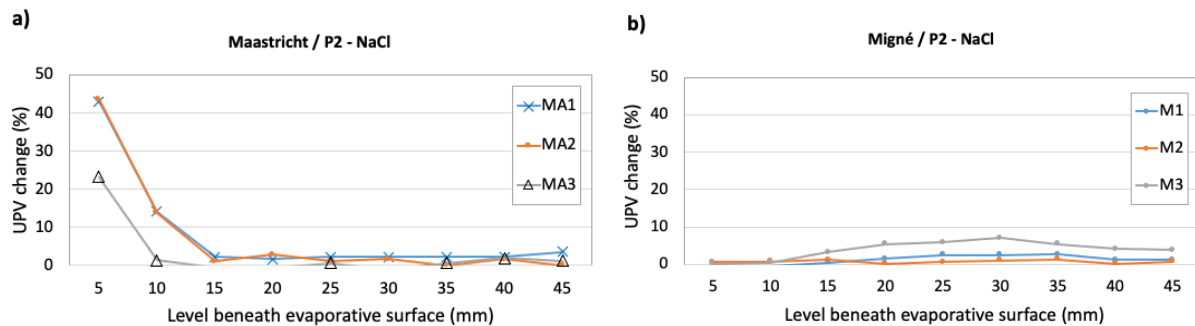


Figure 18: UPV results registered in **NaCl** contaminated specimens with procedure **P2** before and after salt contamination: (a) UPV changes in Maastricht stone measured at 5 mm intervals from the surface, (b) UPV changes in Migné stone measured at 5 mm intervals from the surface.

4. Discussion

Comparison of procedures

A summary of the advantages and disadvantages of the procedures used for salt accumulation (1 wt.% with respect to the total weight of each stone) is presented in Table 4. Procedure **P1-1S** was the most effective in accumulating salts in a thin layer beneath the evaporative surface of the stones without causing too much damage. Rewetting with procedure **P1** led to the damage propagation phase in specimens contaminated with Na_2SO_4 and redistribution of both salts within the specimens, along with the development of salt efflorescence. Procedure **P1-1S** with **NaCl** promoted less salt efflorescence in both stones than with Na_2SO_4 , whereas procedure **P2** caused a higher amount of salt efflorescence in both stones with each of the salts.

The results of the assessment of the salt distribution showed that in all procedures, most of the salt is concentrated in the first millimetres of the subsurface. Stones contaminated with **NaCl** according to procedure **P1-1S** showed higher salt content in the outer layer than stones contaminated with procedure **P2**. In the case of Na_2SO_4 , **P2** induced a higher salt content in the outer layer of both stones.

Mass loss was negligible (lower than 0.05 wt.%) in both materials contaminated with each procedure with **NaCl**. In the case of Na_2SO_4 , slight damage occurred with procedures **P1-S** and **P2**. With procedure **P1**, rewetting caused severe damage in the case of the less porous stone **Migné (P1-1W)** in the form of bursting, whereas Maastricht showed increasingly higher granular disintegration upon rewetting, leading to the conclusion that rewetting triggers damage propagation. The reason for the severe damage

observed in **Migné** after rewetting (**P1-1W**) is probably attributed to a high degree of pore filling after salt contamination (**P1-1S**) and to the development of high stresses in the small pores of this stone after dissolution/recrystallisation of the salt introduced. In the case of **Maastricht**, it can be assumed that the stress developed was not as high since the pores are larger and the resulting pore filling (also with ca. 1 wt.% of salt introduced) is thus lower; consequently, the resulting damage was also less.

The salt types considered in this study follow long-term research studies and recommendations, as presented in the introductory section. The same salt content (1 wt.% of the dry weight of the specimens) was used in all procedures to facilitate comparison. The accumulation procedures were tested in two stones with very similar composition but different porous structure to enable an easier and reliable comparison of the results (e.g., exclude differences in decay which could come from other damage processes, such as chemical reactions, hygric dilation, etc.). Besides, both stones have a unimodal pore size distribution, which simplifies further the comparison. Introducing a realistic salt content into the material and ensuring that the salt accumulates in a thin layer of the material close to the evaporative surface will lead to high salt pore filling. Hence, the damage propagation phase (entailing fast repeated wet-dry cycles) will trigger damage that reproduces onsite salt crystallisation mechanisms. The applicability of the most effective procedure (P1-1S) has been validated by D'Altri et al. [12], who reproduced the protocol by a multiphase numerical model. The numerical model confirmed the results obtained in the two limestones tested and indicated that the procedure is also valid for other types of porous building materials.

Table 4: Advantages and disadvantages of procedures P1 and P2 for accumulating salt in Migné and Maastricht stones.

| Procedure | Advantages | Disadvantages |
|-----------------------|---|---|
| P1-1S | <ul style="list-style-type: none"> - Accumulation of both salts in a thin layer of material (ca. 1 mm) - Low amount of salt efflorescence - Technically easy to perform in a reasonable time | <ul style="list-style-type: none"> - Can cause slight damage with Na₂SO₄ |
| P1-1W & 2W | <ul style="list-style-type: none"> - Rewetting once can promote further accumulation of NaCl in the outer layer of Migné | <ul style="list-style-type: none"> - Can cause medium to high damage with Na₂SO₄ - Can cause redistribution of salt within the specimen thickness - Increases the amount of salt efflorescence - It is more time-consuming than P1-1S |
| P2 | <ul style="list-style-type: none"> - Higher salt enrichment in a thin layer of material (ca. 1 mm) with Na₂SO₄ | <ul style="list-style-type: none"> - Can cause medium damage with Na₂SO₄ - Causes a higher amount of salt efflorescence than P1-1S - Is more time consuming than P1-1S |

Pore clogging and the change of the surface properties due to efflorescence can affect the Stage II drying rate. The different transport properties between Migné and Maastricht, and the different salt solution concentrations used in each stone, are also likely to influence the salt distribution and the resulting pore clogging. Eloukabi et al. [42] studied the effect of NaCl on the drying of porous media. They found that a salt layer on the evaporative surface of a system with a large pore size does not significantly affect the drying rate and can even accelerate it if the pore sizes are sufficiently large. In contrast, a NaCl layer formed on the evaporative surface of porous media with small pore sizes significantly limited the rate of

evaporation. The authors assigned this phenomenon to the fact that, in large pore sized media, the NaCl efflorescence can grow upward, leading to patchy cauliflower efflorescence, as in the case of **Maastricht** contaminated with **NaCl** with procedure **P1-1S** (Figure 4). In contrast, in the case of small pore size media, the salt crystals grow laterally rather than vertically, resulting in a salt crust that may block evaporation, as observed in **Migné** contaminated with **NaCl** with procedure **P1-1S** (Figure 14). This hypothesis is also consistent with the results of the amount of salt efflorescence formed (Figure 6); in general, in the case of **Migné**, there is lower salt efflorescence forming than in **Maastricht**, which indicates a higher amount of subflorescence, thus of pore clogging, hence affecting more severely the drying rate.

Comparison of methods for the analysis of the salt distribution

The salt distribution in the specimens was one of the criteria guiding the choice of the accumulation procedure. Besides, the salt distribution through the depth of the specimen can provide useful information about the risk of damage in salt crystallisation tests: a higher salt accumulation in a thin layer of material close to the evaporative surface implies potentially higher crystallisation pressure and thus a higher risk of damage. Therefore, a reliable measurement of the salt content and distribution is crucial in salt crystallisation tests. In this study, several methods used for assessing the salt distribution have been tested; their advantages and disadvantages, resulting from past experience and from the present research, are summarized in Table 5 and described in detail hereafter.

Table 5: Advantages and disadvantages of each method of analysis used for assessing the salt distribution in **Migné** and **Maastricht** stones.

| Methods | Advantages | Disadvantages |
|----------------|--|---|
| IC | - Very high precision of ion quantity | - Expensive |
| HMC | - Technically simple - Enables the analysis of a large number of samples at the same time - Low cost | - Requires a climatic chamber - Time-consuming - May require further analysis to confirm the results |
| μ-XRF maps | - High precision of salt distribution in the entire sample section | - Expensive and time-consuming sample preparation |
| SEM | - Very high precision of salt distribution - Enables observing the morphology of the salt crystals and the region in which salt crystallizes preferentially | - Representativeness of sample (only small samples can be analysed) - Risk of disturbance of sample condition (salt distribution) during preparation |
| DRMS* & ST | - Good precision on homogeneous samples - Technically simple and fast - Micro-destructive | - DRMS requires performing several measurements for obtaining reliable results - Precision may be affected by the inhomogeneity of the material and the presence of hard minerals or vugs |
| UPV* | - Non-destructive | - Requires a suitable geometry of transducers (pointed shape) - Requires a large number of specimens for obtaining reliable results - Accuracy may depend on stone characteristic and salts |

* Can be performed in situ

HMC is a simple and reliable method for the semi-quantitative analysis of samples contaminated with a single salt and can be used as an alternative or complementary method for more expensive chemical

1
2
3
4 644 analyses, like **IC**. However, care should be taken to monitor precisely the RH inside the climatic chamber
5 645 because a difference of 1% at very high RH, such as 95% RH, can lead to significant differences in the HMC
6 646 values, especially when dealing with high salt contents and very hygroscopic salts, such as NaCl. Hence, in
7 647 the case of NaCl, using an RH of 80% may be advantageous.

9
10 648 **μ-XRF** maps allow for the precise distribution of the salt in a representative section of samples (in this
11 649 study, the entire sample section was mapped). However, it is an expensive and time-consuming type of
12 650 analysis. **SEM** allows the most precise observation of the salt distribution in the pores, including
13 651 information about the preferential location of the salt (e.g., in coarse or finer pores), the crystallisation
14 652 form (e.g., thenardite or mirabilite), and the salt crystallisation habit. The main drawbacks of using SEM
15 653 lie with the sample size and its representativeness, and the disturbance of the sample during preparation.

17 654 The results of **DRMS** and **ST** measurements performed in Migné and Maastricht contaminated according
18 655 to procedure P1 were generally in line with the IC, **μ-XRF**, and SEM results. This confirms that these two
19 656 micro-destructive methods can be successfully used to assess the distribution of salts in stone in a reliable
20 657 way. The DRMS may further be used in-situ, thus providing a useful tool for comparison of laboratory
21 658 results with practice.

24 659 The **UPV** results were in agreement with the results obtained by other techniques in the case of Maastricht
25 660 stone contaminated with NaCl. In contrast, in the case of Migné stone contaminated with NaCl, the UPV
26 661 technique was not able to reveal the accumulation of salts in the outer layer, observed by the other
27 662 investigation techniques. These results suggest that a higher number of specimens should be considered
28 663 for the UPV test to achieve more reliable results because its accuracy may depend on the stone and salt
29 664 type; so, more tests are necessary to define the extent of the applicability of this method for detecting
30 665 the salt distribution.

31 666
32
33
34

35 667 **4. Conclusions**

36
37 668 This study focused on the comparison of two contamination procedures for the accumulation of salts in
38 669 two limestones, as well as on the comparison of different methods for the analysis of salt distribution.

39
40 670 Procedure P1-1S (capillary absorption of a salt solution followed by one drying cycle) proved to be the
41 671 fastest and most effective in accumulating NaCl and Na₂SO₄ in a thin layer of material close to the
42 672 evaporative surface, without resulting in too much salt efflorescence or damage in two types of stone
43 673 with very different porous structure (Maastricht and Migné limestones). Hence, this procedure has been
44 674 selected for reproduction using a multiphase numerical model [12]. The numerical model confirmed the
45 675 obtained results in the tested limestones and indicated that the procedure is also valid for other types of
46 676 porous building materials. Round robin tests with different types of porous building materials are
47 677 currently ongoing to experimentally validate the test and to continue with the damage propagation phase.

50
51 678 All methods used in this study are considered useful for analysing salt distribution. Depending on the aim
52 679 of the analyses, preferences exist. When non-destructive or minimally destructive techniques are to be
53 680 preferred, DRMS, ST, and, with further improvement, UPV can offer a solution for the monitoring of salt
54 681 distribution. If sampling is possible, HMC is a simple technique, not requiring specialized personnel, to
55 682 obtain a reliable indication of the salt content and distribution. When more precise, quantitative
56 683 information on the salt content is needed, IC is the most suitable technique. SEM and **μ-XRF** are most
57 684 useful to provide information about the distribution of salts in pores, their specific location, and
58 685 crystallisation form.

1
2
3
4
5
6
7
8
9
10
11
12
13
14
15
16
17
18
19
20
21
22
23
24
25
26
27
28
29
30
31
32
33
34
35
36
37
38
39
40
41
42
43
44
45
46
47
48
49
50
51
52
53
54
55
56
57
58
59
60
61
62
63
64
65

In general, a combination of screening measurements, carried out by simple and cheap techniques, such as HMC, DRMS, UPV, followed by further analysis on a selection of most relevant samples (chosen based on the results from the screening) with more sophisticated techniques, such as IC, SEM, and μ -XRF seems to be the most suitable and sustainable choice.

The future work of the TC ASC-271 will focus on the propagation phase. Round robin tests with other types of porous building materials are currently ongoing.

CRedit authorship contribution statement

Cristiana Nunes: Methodology, Experimental part - accumulation test, Data curation, Writing - original draft. **Asel Maria Aguilar Sanchez:** Methodology, Experimental part - μ -XRF maps and SEM, Data curation. **Sebastiaan Godts:** Methodology, Experimental part - IC and HMC, Data curation. **Davide Gulotta:** Methodology, Experimental part - SEM, Data curation. **Ioannis Ioannou:** Methodology, Experimental part - DRMS and ST, Data curation, Review. **Barbara Lubelli:** Methodology, Writing - review, Project coordination. **Beatriz Menendez:** Methodology, Experimental part - UPV, Data curation. **Noushine Shahidzadeh:** Methodology, Experimental part - SEM, Review. **Zuzana Slížková:** Methodology, Experimental part - UPV, Data curation. **Magdalini Theodoridou:** Methodology, Experimental part - DRMS, and ST.

Declaration of Competing Interest

The authors declare that they have no known competing financial interests or personal relationships that could have appeared to influence the work reported in this paper.

Acknowledgements

All authors acknowledge Kévin Beck for providing the characterisation of the stones and Véronique Vergès-Belmin for providing the stone specimens used in this study. All authors also thank Rob Van Hees for a thorough reading and helpful comments on the paper. The authors are also thankful to all the other RILEM TC ASC-271 members for their contribution in discussions, especially Tim De Kock and Julie Desarnaud, who have performed relevant experiments for future work.

Cristiana Nunes thanks Kateřina Mlsnová for helping with the specimens' preparation for the contamination procedures. Sebastiaan Godts acknowledges Mohamed Rich, Xavier Monfort, and graduate interns Simone Semprini, Elien Decaesteker, and Alice Vrancken for their help with sample preparation, IC, and HMC analysis. Ioannis Ioannou thanks RILEM member Loucas Kyriakou for his help with the ST and DRMS tests. Zuzana Slížková acknowledges Marek Eisler for performing the UPV analysis.

Three anonymous reviewers provided valuable comments to improve the paper.

1
2
3
4 **725 References**

- 5
6 726 [1] Alves C, Figueiredo C, Sanjurjo-Sánchez J (2020) Rock Features and Alteration of Stone Materials Used for
7 727 the Built Environment: A Review of Recent Publications on Ageing Tests, *Geosciences* 10
8 728 (3). <https://doi.org/10.3390/geosciences10030091>
9
10 729 [2] Lubelli B, Cnudde V, Diaz-Goncalves T, Franzoni E, Van Hees RP, Ioannou I, Menendez B, Nunes c, Siedel H,
11 730 Stefanidou M, Verges-Belmin V, Viles H (2018) Towards a more effective and reliable salt crystallisation test for
12 731 porous building materials: state of the art. *Mater Struct* 51 (2). <http://dx.doi.org/10.1617/s11527-018-1180-5>.
13
14 732 [3] CEN (1999) EN 12370 Natural stone test methods. Determination of resistance to salt crystallisation.
15
16 733 [4] RILEM (1980) Recommended tests to measure the deterioration of stone and to assess the effectiveness of
17 734 treatment methods, Test V.1a—crystallisation test by total immersion (for untreated stone); Test V.1b—
18 735 crystallisation test by total immersion (for treated stone); Test V.2— crystallisation test by partial immersion.
19 736 *Mater Struct* 13(75):175–253
20
21 737 [5] RILEM TC 127-MS (1998) MS-A.1— determination of the resistance of wallettes against sulphates and
22 738 chlorides. *Mater Struct* 31:2–9
23
24 739 [6] RILEM TC 127-MS (1998) MS-A.2— uni-directional salt crystallisation test for masonry units. *Mater Struct*
25 740 31:10–11
26
27 741 [7] WTA Merkblatt 2-9-04/D (2005) Sanierputzsysteme/ Renovation mortar systems. WTA Publications,
28 742 Stuttgart
29
30 743 [8] CEN (2003) EN 14147 Natural stone test methods - Determination of resistance to ageing by salt mist.
31
32 744 [9] ASTM B117-03 (2003) Standard Practice for Operating Salt Spray (Fog) Apparatus.
33
34 745 [10] Tuutti K (1982) Corrosion of steel in concrete. CBI Forsk. 824. <http://lup.lub.lu.se/record/3173286>
36 746 (accessed May, 2020).
37
38 747 [11] Flatt R, et al. (2017) Predicting salt damage in practice: A theoretical insight into laboratory tests. *RILEM*
39 748 *Technical Letters* (2) 108–118. <http://dx.doi.org/10.21809/rilemtechlett.2017.41>.
40
41 749 [12] D'Altri AM, de Miranda S, Beck K, De Kock T, Derluyn H (submitted to publication in the *Construction and*
42 750 *Building Materials journal*) Towards a more effective and reliable salt crystallisation test for porous building
43 751 materials. Part II: Predictive modelling of salt distribution
44
45 752 [13] Angeli M, Benavente D, Bigas J-P, Menendez B, Hebert R, David C (2007) Modification of the porous
46 753 network by salt crystallisation in experimentally weathered sedimentary stones. *Mater Struct* 41 (6): 1091–
47 754 1108. <https://doi.org/10.1617/s11527-007-9308-z>
48
49 755 [14] Beck K, Al-Mukhtar M (2010) Evaluation of the compatibility of building limestones from salt crystallisation
50 756 experiments. *Geol Soc Lond Spec Publ* 333 (1):111–118. <https://doi.org/10.1144/sp333.11>
51
52 757 [15] Shahidzadeh-Bonn, N, Desarnaud J, Bertrand F, Château X, Bonn D (2010) Damage in Porous media due
53 758 to salt crystallisation, *Physical Review E* 81 (6) 066110. <https://doi.org/10.1103/physreve.81.066110>
54
55 759 [16] Ioannou I, Hall C, Hoff WD, Pugsley VA, Jacques SDM (2005) Synchrotron radiation energy-dispersive X-ray
56 760 diffraction analysis of salt distribution in Lépine limestone, *Analyst* 130, <https://doi.org/10.1039/b504274g>
57
58
59
60
61
62
63
64
65

1
2
3
4
5
6
7
8
9
10
11
12
13
14
15
16
17
18
19
20
21
22
23
24
25
26
27
28
29
30
31
32
33
34
35
36
37
38
39
40
41
42
43
44
45
46
47
48
49
50
51
52
53
54
55
56
57
58
59
60
61
62
63
64
65

[17] Derluyn H, Vontobel P, Mannes D, Derome D, Lehmann E, Carmeliet J (2019) Saline water evaporation and crystallization-induced deformations in building stone: insights from high-resolution neutron radiography, *Transport in Porous Media*, 128(3): 895-913. <http://dx.doi.org/10.1007/s11242-018-1151-x>.

[18] Goudie AS (1986) Laboratory simulation of "the wick effect" in salt weathering of rock. *Earth Surf Proc Land* 11(3):275–285. <https://doi.org/10.1002/esp.3290110305>

[19] Rodriguez-Navarro C, Doehne E (1999) Salt weathering: influence of evaporation rate, supersaturation and crystallisation pattern, *Earth Surface Processes and Landforms* 24 (3). [https://doi.org/10.1002/\(sici\)1096-9837\(199903\)24:3<191::aid-esp942>3.0.co;2-g](https://doi.org/10.1002/(sici)1096-9837(199903)24:3<191::aid-esp942>3.0.co;2-g)

[20] Benavente D, Garcia del Cura M, Bernabeu A, Ordonez S (2001) Quantification of salt weathering in porous stones using an experimental continuous partial immersion method. *Eng Geol* 59 (3–4):313–325. [https://doi.org/10.1016/s0013-7952\(01\)00020-5](https://doi.org/10.1016/s0013-7952(01)00020-5)

[21] Modestou S, Ioannou I (2017) Tracing the salt crystallisation front in limestone using the DRMS. In: Papamichos E, Papanastasiou P, Pasternak E, Dyskin A (eds.) *Bifurcation and degradation of geomaterials with engineering applications*. Springer Series in Geomechanics and Geoengineering. DOI 10.1007/978-3-319-56397-8_33

[22] Benavente D, Garcia del Cura M, Bernabeu A, Ordonez S (2001) Quantification of salt weathering in porous stones using an experimental continuous partial immersion method. *Eng Geol* 59 (3–4) 313–325. [https://doi.org/10.1016/s0013-7952\(01\)00020-594](https://doi.org/10.1016/s0013-7952(01)00020-594).

[23] Nogueira R, Ferreira Pinto AP, Gomes A (2020) Artificial ageing by salt crystallization: test protocol and salt distribution patterns in lime-based rendering mortars. *J Cultural Heritage*, <https://doi.org/10.1016/j.culher.2020.01.013>

[24] Lopez-Arce P, Tagnit-Hammou M, Menendez B, Mertz J-D, Kaci A (2016) Durability of stone-repair mortars used in historic buildings from Paris. *Mater Struct* 49 (12) 5097–5115. <https://doi.org/10.1617/s11527-016-0846-0>

[25] Nunes C, Skruzna O, Válek J (2018) Study of nitrate contaminated samples from a historic building with the hygroscopic moisture content method: Contribution of laboratory data to interpret results practical significance. *J Cult Herit* 30, 57-69. <https://doi.org/10.1016/j.culher.2017.09.013>

[26] Menendez B, Petranova V (2016) Effect of mixed vs single brine composition on salt weathering in porous carbonate building stones for different environmental conditions. *Eng Geol* 210, 124–139. <https://doi.org/10.1016/j.enggeo.2016.06.011>

[27] Cardell C, Benavente D, Rodríguez-Gordillo J (2008) Weathering of limestone building material by mixed sulfate solutions. Characterization of stone microstructure, reaction products and decay forms. *Materials Characterization* 59 (10) 1371–1385. <http://dx.doi.org/10.1016/j.matchar.2007.12.003>.

[28] Ruiz-Agudo E, Mees F, Jacobs P, Rodriguez-Navarro C (2007) The role of saline solution properties on porous limestone salt weathering by magnesium and sodium sulfates. *Environ Geol* 52 (2) 269–281. <https://doi.org/10.1007/s00254-006-0476-x>

[29] MacWilliam K, Nunes C (2019) Towards a More Realistic and Effective Use of Sodium Sulfate in Accelerated Ageing of Natural Stone. *Structural Analysis of Historical Constructions, 1949–1958*. http://dx.doi.org/10.1007/978-3-319-99441-3_209.

[30] Godts S, Hayen R, De Clercq H (2014) Common salt mixtures database: a tool to identify research needs. In: De Clercq (ed.) *Proc. 3rd International Conference on Salt Weathering of Buildings and Stone Sculptures*. Brussels: KIK-IRPA, 185-198.

1
2
3
4
5
6
7
8
9
10
11
12
13
14
15
16
17
18
19
20
21
22
23
24
25
26
27
28
29
30
31
32
33
34
35
36
37
38
39
40
41
42
43
44
45
46
47
48
49
50
51
52
53
54
55
56
57
58
59
60
61
62
63
64
65

[31] Benavente D, García del Cura MA, Fort R, Ordóñez S (2004) Durability estimation of porous building stones from pore structure and strength. *Eng Geol* 74 (1-2): 113–27. <http://dx.doi.org/10.1016/j.enggeo.2004.03.005>

[32] Desarnaud J, Bertrand F, Shahidzadeh-Bonn N (2013) Impact of the kinetics of salt crystallisation on stone damage during rewetting/drying and humidity cycling, *J Applied Mechanics* 80 (2). <https://doi.org/10.1115/1.4007924>

[33] Benson PM, Meredith PG, Platzman ES, and White RE (2005) Pore fabric shape anisotropy in porous sandstones and its relation to elastic wave velocity and permeability anisotropy under hydrostatic pressure, *Int J Rock Mech Min Sci* 42: 890-899. <https://doi.org/10.1016/j.ijrmms.2005.05.003>

[34] Aly N, Hamed A, Gomez-Heras M, Benavente D, and Alvarez de Buergo M (2016) The Effect of Salt Crystallisation on the Mechanical Properties of Limestone: Statistical Correlation between Non-destructive and Destructive Techniques, in Hughes JJ and Howind T (Eds.), *Proc. 13th Int. Cong. on the Deterioration and Conservation of Stone*, Paisley: University of the West of Scotland, 225-231

[35] Modestou S, Theodoridou M, Ioannou I (2015) Micro-destructive mapping of the salt crystallisation front in limestone. *Eng Geol* 193:337–347. <https://doi.org/10.1016/j.enggeo.2015.05.008>

[36] Theodoridou M, Dagrain F, Ioannou I (2015) Micro-destructive cutting techniques for the characterization of natural limestone. *International Journal of Rock Mechanics and Mining Sciences* 76: 98-103. <http://dx.doi.org/10.1016/j.ijrmms.2015.02.012>

[37] Diaz Goncalves T, Delgado Rodrigues J (2006) Evaluating the salt content of salt-contaminated samples on the basis of their hygroscopic behaviour, Part I: fundamentals, scope and accuracy of the method, *J. Cult. Herit.* 7, 79–84. <http://dx.doi.org/10.1016/j.culher.2006.02.009>

[38] Nasraoui M, Nowik W, Lubelli B (2009) A comparative study of hygroscopic moisture content, electrical conductivity and ion chromatography for salt assessment in plasters of historical buildings. *Constr Build Mater* 23 (5): 1731-1735. <https://doi.org/10.1016/j.conbuildmat.2008.09.029>

[39] Price C (Ed.) (2000) *An expert chemical model for determining the environmental conditions needed to prevent salt damage in porous materials*, European Commission Research Report No 11, (Protection and Conservation of European Cultural Heritage). London: Archetype Publications

[40] ICOMOS-ISCS (2008) *Illustrated glossary on stone deterioration patterns*. Ateliers 30 Impression, Champigny/Marne.

[41] Monument Diagnosis and Conservation System. <https://mdcs.monumentenkenis.nl/> (accessed May 2020)

[42] Eloukabi H, Sghaier N, Ben Nasrallah S, Prat M (2013) Experimental study of the effect of sodium chloride on drying of porous media: The crusty–patchy efflorescence transition. *Int J Heat and Mass Transfer* 56 (1-2). <http://dx.doi.org/10.1016/j.ijheatmasstransfer.2012.09.045>